

1 **Chesapeake Bay nitrogen fluxes derived from a land-estuarine ocean**
2 **biogeochemical modeling system: Model description, evaluation and nitrogen**
3 **budgets**

4
5 Submitted to the special issue of Journal of Geophysical Research – Biogeosciences
6 devoted to “Land-ocean Interactions in Coastal Margin Systems”

7
8
9 Yang Feng¹, Marjorie A. M. Friedrichs¹, John Wilkin², Hanqin Tian³, Qichun Yang³,
10 Eileen E. Hofmann⁴, Jerry D. Wiggert⁵ and Raleigh R. Hood⁶

11
12
13 ¹Virginia Institute of Marine Science, College of William and Mary, Gloucester Point, Virginia

14 ²Institute of Marine and Coastal Sciences, Rutgers University, New Brunswick, New Jersey

15 ³International Center for Climate and Global Change Research and School of Forestry and
16 Wildlife Sciences, Auburn University, Auburn, Alabama

17 ⁴Center for Coastal Physical Oceanography, Old Dominion University, Norfolk, Virginia

18 ⁵Department of Marine Science, University of Southern Mississippi, Stennis Space Center,
19 Mississippi

20 ⁶Horn Point Laboratory, University of Maryland Center for Environmental Science, Cambridge,
21 Maryland

22
23

24 **Abstract**

25 The Chesapeake Bay plays an important role in transforming riverine nutrients before
26 they are exported to the adjacent continental shelf. Although the mean nitrogen budget of
27 the Chesapeake Bay has been previously estimated from observations, uncertainties
28 associated with interannually varying hydrological conditions remain. In this study, a
29 land-estuarine-ocean biogeochemical modeling system is developed to quantify
30 Chesapeake riverine nitrogen inputs, within-estuary nitrogen transformation processes
31 and the ultimate export of nitrogen to the coastal ocean. Model skill was evaluated using
32 extensive in situ and satellite-derived data, and a simulation using environmental
33 conditions for 2001-2005 was conducted to quantify the Chesapeake Bay nitrogen
34 budget. The five-year simulation was characterized by large riverine inputs of nitrogen
35 ($154 \times 10^9 \text{ gN y}^{-1}$) split roughly 60:40 between inorganic:organic components. Much of
36 this was denitrified ($34 \times 10^9 \text{ gN y}^{-1}$) and buried ($46 \times 10^9 \text{ gN y}^{-1}$) within the estuarine
37 system. A positive net annual ecosystem production for the Bay further contributed to a
38 large advective export of organic nitrogen to the shelf ($91 \times 10^9 \text{ gN y}^{-1}$) and negligible
39 inorganic nitrogen export. Interannual variability was strong, particularly for the riverine
40 nitrogen fluxes. In years with higher than average riverine nitrogen inputs, most of this
41 excess nitrogen (50-60%) was exported from the Bay as organic nitrogen, with the
42 remaining split between burial, denitrification and inorganic export to the coastal ocean.
43 In comparison to previous simulations using generic shelf biogeochemical model
44 formulations inside the estuary, the estuarine biogeochemical model described here
45 produced more realistic and significantly greater exports of organic nitrogen and lower
46 exports of inorganic nitrogen to the shelf.

47 **1. Introduction**

48 Located at the intersection between land and ocean, estuaries play an important
49 role in global carbon and biogeochemical cycles [*Bauer et al.*, 2013; *Bianchi and Bauer*,
50 2011, *Canuel et al.*, 2012]. Chesapeake Bay, the largest estuary in the United States,
51 plays a particularly significant role in the transformation and burial of riverine terrestrial
52 nitrogen [*Bronk et al.*, 1998; *Glibert et al.*, 1991; *Horrigan et al.*, 1990; *Kemp*, 2005]. As
53 a result, it significantly impacts the form and amount of nitrogen that is exported from
54 riverine sources to the adjacent continental shelf.

55 The fate of riverine nutrients has been intensely studied in the Chesapeake Bay
56 where available water quality data extend back to 1950 [*Flemer et al.*, 1983]. Using five
57 early years (1977-1982) of U.S. Environmental Protection Agency (EPA) data, *Smullen*
58 *et al.* [1982] concluded that the Chesapeake Bay retained almost all the nutrients entering
59 during this time period. Using the same data *Nixon et al.* [1987] reassessed the nitrogen
60 budget and concluded that the Bay retained only a small amount (3-6%) of the nitrogen
61 entering the system. In a third study, *Fisher et al.* [1988] developed a conceptual model
62 suggesting roughly 50% of total nitrogen left the Bay, primarily through phytoplankton
63 sinking. In these early studies the relative amount of riverine total nitrogen loss in the
64 Bay and export to the open ocean were quite controversial, primarily because of the
65 limited availability of observations and the different assumptions and approaches
66 employed.

67 A more consistent Chesapeake Bay nitrogen budget came together in the 1990's,
68 after additional measurements were available. *Boynton et al.* [1995] calculated that about
69 70% of the nitrogen entering the Bay was lost to denitrification, burial and fisheries

70 harvest, and the remaining 30% was exported to the open ocean. However, these
71 calculations did not include a separation of nitrogen between inorganic and organic
72 forms, and the nitrogen exchange between the Bay and the adjacent shelf was calculated
73 from subtracting the Bay internal sinks from riverine and atmospheric sources, rather
74 than from direct measurements or modeling results. A more detailed budget was
75 described by *Kemp et al.* [1997], however this budget was limited to the main stem of the
76 Bay (Fig. 1). In these calculations nitrogen was separated into dissolved inorganic and
77 organic forms, and the nitrogen seaward transport was calculated from a model
78 simulation. They concluded that roughly 75% of the nitrogen entering the mainstem of
79 the Bay was exported to the open ocean. In addition, the ratio of dissolved inorganic
80 nitrogen to total organic nitrogen at the Bay mouth (0.04) was much smaller than that at
81 the head of the Bay (5.1). Overall the net ecosystem production in the main stem of the
82 Bay was positive, leading *Kemp et al.* [1997] to conclude that this portion of the Bay is
83 net autotrophic.

84 Although nitrogen budget estimates from observational studies such as those
85 described above have been becoming more consistent in recent decades, they are still
86 associated with considerable uncertainties, largely resulting from relatively low temporal
87 and spatial sampling frequency as well as the interannual variability associated with the
88 observations. One issue with these previous nitrogen budget estimates, for example, is
89 that due to data limitations, asynchronous observations had to be combined. In *Kemp et al.*
90 [1997] nitrogen exchanges at the Bay mouth were from the year 1986, but net ecosystem
91 production (called net ecosystem metabolism in their paper) was from a multiple year
92 average (1986-1993). In addition, to avoid variation of fluxes with different hydrological

93 conditions, *Kemp et al.* [1997] and *Boynton et al.* [1995] both remove years with extreme
94 wet or dry conditions and use years with low to moderate river flow only.

95 In order to examine how interannually varying riverine inputs of nitrogen to
96 Chesapeake Bay affect estuarine nitrogen fluxes, a land-estuarine-ocean biogeochemical
97 modeling system is developed for this region. Riverine inputs of nitrogen to the Bay are
98 computed from a terrestrial ecosystem model that resolves riverine discharge variability
99 on scales of days to years. This temporally varying discharge is then used as input to the
100 estuarine-biogeochemical model, which provides estimates of the nitrogen fluxes within
101 the Bay as well as advective exports from the Bay to the adjacent Mid-Atlantic Bight
102 shelf. This coupled modeling system calculates the nitrogen budget of the Chesapeake
103 Bay for a continuous 5-year period (2001-2005), of which the first two years (2001 and
104 2002) were dry flow years, the third year (2003) was a wet flow year, and the last two
105 years (2004 and 2005) were intermediate flow years.

106 The content of this paper is organized as follows. Section 2 and the associated
107 supporting information S1 present a complete description of our land-estuarine-
108 biogeochemistry modeling system and the configuration implemented here. In Section 3,
109 model skill is evaluated relative to extensive data from the Chesapeake Bay Program as
110 well as satellite ocean color data. In Section 4, a simulated nitrogen budget for the Bay is
111 presented and compared to previous budgets derived using observational data as well as
112 model results using a generic basin-scale continental shelf model. A summary of our
113 results and potential future work is provided in Section 5.

114 **2. Model Description**

115 **2.1 Hydrodynamic Model: ROMS**

116 The physical component of the coupled model is based on the Regional Ocean
117 Modeling System (ROMS) [*Shchepetkin and McWilliams, 2005*] version 3.6. The model
118 domain and horizontal grid follows the Chesapeake Bay community implementation of
119 the ROMS (ChesROMS) [*Brown et al., 2013; Xu et al., 2012*]. The domain spans the
120 region from 77.2°W to 75.0°W and from 36°N to 40°N, covering the main stem and
121 primary tributaries of the Chesapeake Bay, as well as part of the mid-Atlantic Bight (Fig.
122 1). The horizontal grid spacing varies with highest resolution (430 m) in the northern Bay
123 near the Chesapeake and Delaware Canal, lowest resolution (~10 km) in the southern end
124 of the mid-Atlantic Bight, and an average grid spacing within the Chesapeake Bay of 1.7
125 km. As in ChesROMS, the model has 20 terrain-following vertical layers with higher
126 resolution near the surface and bottom boundaries. However, unlike ChesROMS, the
127 vertical s-coordinate function follows *Shchepetkin and Williams [2009]*, and stretching
128 parameters at the surface and bottom are set to 6.0 and 4.0, respectively. The bottom
129 topography is also slightly smoothed as in *Scully [2013]* to avoid pressure gradient errors
130 caused by steep bathymetry.

131 The model is forced with spatially uniform but temporally varying winds,
132 measured every hour at the Thomas Point Light Buoy (-76.4°W, 38.9°N). These observed
133 winds are used rather than other wind products such as those derived from the North
134 American Regional Reanalysis (NARR), since the latter underestimates the observed
135 summer winds by roughly 30%, and does not show the strong directional asymmetry that
136 may play a key role in modulating the strength of vertical mixing [*Scully, 2013*]. Other
137 atmospheric forcing, including air temperature, relative humidity, pressure, precipitation,
138 long and shortwave radiation were obtained from NARR with 3-hr time resolution. The

139 NARR shortwave radiation was found to be systematically higher than adjacent buoy
140 observations, and therefore it was reduced by 80% [Wang *et al.*, 2012]. At the open
141 boundary, the model is forced by open ocean tides and non-tidal water levels as in
142 ChesROMS [Xu *et al.*, 2012].

143 The model is configured to use the recursive MPDATA 3D advection scheme for
144 tracers, 3rd-order upstream advection scheme for 3D horizontal momentum and 4th-order
145 centered difference for 3D momentum in the vertical. The Generic Length-Scale vertical
146 turbulent mixing scheme [Warner *et al.*, 2005b] is implemented with the stability
147 functions of Kantha and Clayson [1994], and background mixing coefficients for both
148 momentum and tracers are set to $10^{-5} \text{ m}^2 \text{ s}^{-1}$ as in Scully [2010].

149 **2.2 Biogeochemical Model: ECB**

150 The Estuarine-Carbon-Biogeochemistry (ECB) model implemented here includes
151 a simplified nitrogen cycle with eleven state variables (Fig. 2b): nitrate ($[\text{NO}_3]$),
152 ammonium ($[\text{NH}_4]$), phytoplankton (P), zooplankton (Z), small and large detritus (D_S and
153 D_L), semi-labile and refractory dissolved organic nitrogen ($[\text{DON}]_{\text{SL}}$ and $[\text{DON}]_{\text{RF}}$),
154 inorganic suspended solids ($[\text{ISS}]$), chlorophyll ($[\text{Chl}]$) and oxygen ($[\text{O}_2]$). Although
155 analogous carbon state variables are included in the model as well (dissolved organic
156 carbon, detrital carbon and dissolved inorganic carbon), these will be described and
157 analyzed in a separate publication.

158 All state variables are horizontally and vertically advected and diffused along
159 with the physical circulation variables. The biological source/sink terms, functions and
160 parameter values are presented in supporting information S1. The model structure was
161 based on Druon *et al.* [2010], which was originally derived from Fennel *et al.* [2006],

162 with modifications similar to those described by *Hofmann et al.* [2008, 2011]. However,
163 these models were all designed for coastal applications. To adapt the model to an
164 estuarine application in the Chesapeake Bay, a number of model formulations were
165 modified, as described below.

166 **2.2.1 Refractory and Semi-labile DON**

167 Since dissolved organic nitrogen plays a critical role in estuarine nitrogen cycling
168 processes [*Keller and Hood, 2011*], semi-labile and refractory DON components are
169 included as separate state variables in the model. Although $[DON]_{RF}$ does not participate
170 actively in any biological processes, it is input from the rivers, and transported via
171 advection and diffusion throughout the model domain and reduces the light intensity. The
172 $[DON]_{SL}$ is derived from phytoplankton exudation, sloppy feeding and detrital
173 solubilization, and is remineralized into NH_4 (Supporting Information S1).

174 **2.2.2 Inorganic Suspended Solids**

175 As the refractory DON, inorganic suspended solids (ISS) do not participate in the
176 nitrogen cycling directly, but play an important role in reducing the light intensity in the
177 northern Chesapeake Bay. The ISS formulation and related parameters follow *Xu and*
178 *Hood* [2006]. Specifically, ISS is introduced as an additional state variable, which is
179 decreased by water column sinking and increased by bottom resuspension (Supporting
180 Information S1).

181 **2.2.3 Light Attenuation**

182 The photosynthetic available radiation decreases exponentially with water depth:

183
$$I(z) = I_0 \cdot PARfrac \cdot e^{-zK_D}$$

184 where I_0 is the light just below the sea surface, $PARfrac$ is the fraction of light that is
185 available for photosynthesis, K_D is the diffuse attenuation coefficient, and z is depth. *Xu*
186 *et al.* [2005] used chlorophyll, total suspended solids (TSS), and surface salinity to
187 specify K_D for the Chesapeake Bay, where salinity was used as a proxy for chromophoric
188 dissolved organic matter (CDOM), since CDOM is generally inversely related to salinity.
189 To avoid K_D becoming negative in high salinity regimes, *Xu et al.* [2005] identified
190 empirical relations for high (≥ 15 psu) and low (≤ 15 psu) salinity regimes, respectively.
191 They found that their model successfully explained 70% of the observed K_D variability in
192 the Chesapeake Bay. However, their empirical relationship was based on Chesapeake
193 Bay Program observations from 1995 and 1996, which is outside the more recent study
194 period used in this analysis. Therefore, as a part of this analysis their method was
195 repeated using observations from 2000-2005, and resulted in the following empirical
196 relationship:

$$197 \quad K_D = 1.4 + 0.063[TSS] - 0.057S$$

198 where TSS [in mg L^{-1}] represents total suspended solids, including both the inorganic
199 suspended solids (section 2.1.2.1) and organic suspended solids (defined here as
200 particulate organic nitrogen (PON) including P, Z, D_S , and D_L). This relationship was
201 found to explain 76% of the observed variability in K_D . Chlorophyll was excluded from
202 the relationship, as it did not successfully explain any significant additional variability
203 [*Feng et al.*, in prep.]. With this single relationship, K_D is positive when salinity is less
204 than ~ 24 PSU, which covers almost the entire Chesapeake Bay. In high salinity regions
205 of the model domain (close to the Bay mouth and on the Mid-Atlantic Bight shelf) it is
206 possible for the right hand side of the above equation to become negative. To prevent

207 this, the configuration of K_D used for the U.S East Coast shelf model [*Friedrichs et al.*, in
208 prep. for this issue], is used in high salinity regimes:

209 If $1.4 + 0.063[TSS] - 0.057S < 0$, then

210
$$K_D = 0.04 + 0.02486[Chl] + 0.003786 \{0, 6.625[DON] - 70.819\}_{\max}$$

211 where [DON] represents total DON, i.e. the sum of both refractory and semi-labile
212 components.

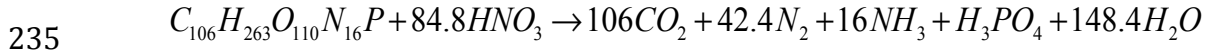
213 **2.2.4 Phytoplankton Specific Growth Rate**

214 *Druon et al.* [2010] found that using a temperature-independent maximum
215 specific growth rate ($\mu_{\max} = 1.6 \text{ d}^{-1}$) substantially improved their model results in the Mid-
216 Atlantic Bight (their Supporting Information S1, Table S2). In their Chesapeake Bay
217 biogeochemical model, *Xu and Hood* [2006] also used constant (temperature-
218 independent) specific growth rates for phytoplankton species, but imposed different
219 values for phytoplankton adapted to low salinity ($\mu_{\max} = 0.96 \text{ d}^{-1}$) versus high salinity (
220 $\mu_{\max} = 3.22 \text{ d}^{-1}$) regions. Here, a constant maximum specific growth rate (2.15 d^{-1}) is used
221 for our single phytoplankton state variable, based on information provided by *Li et al.*
222 [2009] for the Chesapeake Bay.

223 **2.2.5 Water Column Denitrification**

224 One of the most significant differences between the ECB model and model
225 implementations for the continental shelf results from the fact that hypoxia can occur in
226 estuarine sub-pycnocline waters when water column stratification prevents re-aeration of
227 deeper waters [*Hagy et al.*, 2004; *Bever et al.*, 2013]. During such periods,
228 remineralization of organic matter in the water column transitions from an aerobic to an
229 anaerobic process via facultative anaerobes that shift to suitable alternative electron

230 acceptors such as nitrate or nitrite [King, 2005]. Water column denitrification has
 231 previously been considered in marine ecosystem models of other hypoxic systems, such
 232 as the Black Sea and Arabian Sea [Oguz, 2002; Resplandy et al., 2012]. The
 233 stoichiometric equation for oceanic denitrification first proposed by Richards [1965]
 234 follows:



236 where organic matter is reduced and dinitrogen gas is released to the atmosphere, a
 237 process that has global N-cycle implications [e.g., Codispoti et al., 2001].

238 Within the ROMS-ECB implementation, onset of water column denitrification is
 239 associated with decreasing dissolved oxygen concentration, which reflects the known
 240 oxic repression of nitrogen oxide reductases that are needed to catalyze denitrification
 241 reactions [Hood et al., 2006]. With these issues in mind and following Oguz [2002],
 242 nitrate loss during water column denitrification is modeled as:

$$243 \quad \left. \frac{\partial [NO_3]}{\partial t} \right|_{WC-DNF} = -\eta_{DNF} [f_{DNF}, f_{WC}]_{\min} \left\{ (1 - \delta_N) (r_{D_S} D_S + r_{D_L} D_L) + r_{[DON]} e^{\kappa_{[DON]} T} [DON] \right\}$$

244 where $f_{DNF} = \frac{K_{DNF}}{O_2 + K_{DNF}}$ and $f_{WC} = \frac{[NO_3]}{[NO_3] + K_{WNO_3}}$ are the oxygen and nitrate limitation

245 terms, respectively, for denitrification. The latter limitation is imposed to prevent
 246 generation of negative nitrate concentrations. In this way, water column denitrification
 247 depends on the stoichiometry for remineralization via denitrification (η_{DNF}), the half-
 248 saturation constant for water column denitrification (K_{DNF}), as well as the half-saturation
 249 constant for water column NO_3 uptake shutting down (K_{WNO_3}).

250 2.2.6 Oxygen Limitation of Remineralization

251 In the water column, oxygen concentration also regulates the rate of nitrification,
252 but in an inverse fashion as compared to its influence on denitrification: as denitrification
253 is enhanced, nitrification is diminished. Thus the nitrification limitation term in the ECB
254 model takes the form:

255
$$f_{NTR} = \frac{O_2}{O_2 + K_{NTR}}$$

256 where K_{NTR} is the half-saturation constant for water column nitrification. The
257 remineralization rate of organic matter is regulated by the combined rates of nitrification
258 and denitrification; therefore, the summation of f_{NTR} and f_{DNF} is included for all terms
259 associated with remineralization. The factors f_{NTR} and f_{DNF} are then used to partition
260 aerobic and anaerobic bacterial processing of organic matter between consumption of
261 oxygen and nitrate, respectively.

262 **2.3 Riverine Inputs**

263 In this implementation, ROMS-ECB is forced with daily riverine nutrient input
264 derived from the Dynamic Land Ecosystem Model (DLEM), including NO_3 , NH_4 , DON
265 and PON as well as daily freshwater discharge (Fig. 2a). DLEM is a grid-based fully
266 distributed model which couples major biogeochemical cycles, the water cycle, and
267 vegetation dynamics to derive temporally and spatially explicit estimates of fluxes of
268 water, greenhouse gases and carbon and nitrogen storage in terrestrial ecosystems (*Tian*
269 *et al.*, 2010, 2014; *Liu et al.*, 2013]. DLEM has been used to hindcast riverine discharge
270 of freshwater, nutrients and organic matter to the U.S. eastern continental shelf over the
271 past century [*Yang et al.*, 2014a,b] and forecast these fluxes over the 21st century [*Tao et*
272 *al.*, 2014]. The model incorporates hydrological components to simulate lateral water flux
273 from terrestrial ecosystems to river networks. Export of freshwater from land surface to

274 coastal areas is simulated through three major processes: generation of surface runoff
275 after rainfall events, the leaching of water from land to river networks in the form of
276 overland flow and base flow, and the flow routing process along river channels from
277 upstream areas to coastal regions. For ease of computing in the estuarine model, the total
278 export to the Chesapeake Bay computed by DLEM, including groundwater discharge,
279 was apportioned to ten tributaries, and entered the model domain at these ten locations
280 (Fig. 1a). Because DON provided by DLEM was not separated into semi-labile and
281 refractory components, assumptions had to be made regarding the relative proportions of
282 each component. Of the total DON entering the Bay, 50% was assumed to be semi-labile,
283 and 20% was assumed to be refractory. The remaining 30% of the DON leaving the
284 rivers was assumed to flocculate and be buried before reaching the 5 psu isohaline [*Bronk*
285 *et al.*, 1998]. The PON provided by DLEM was assumed to enter the Bay entirely as
286 small detritus.

287 In addition to the above nitrogen components, the river forcing of the model
288 requires temperature and salinity, which was calculated from climatological USGS data
289 (1980 to 2011), and oxygen, which was assumed to be at saturation and computed as a
290 function of temperature and salinity [*Weiss*, 1970]. The concentration of other river
291 variables, including phytoplankton ($1.8 \text{ mmole-N m}^{-3}$), zooplankton ($0.06 \text{ mmole-N m}^{-3}$)
292 and chlorophyll ($6.0 \text{ mg-Chl m}^{-3}$), were input to the model domain as uniform
293 concentrations.

294 **2.4 Model Implementation**

295 At the open boundary, the *Chapman* [1985] condition is used for the free surface,
296 the radiation condition is used for tracers and baroclinic 3D velocities and the *Flather*

297 [1976] condition is used for barotropic 2D velocities. Temperature and salinity are
298 nudged in and out of the model domain to climatological data fields generated from the
299 2001 World Ocean Atlas with time scales of 2-hr and 2 day, respectively [Marchesiello *et*
300 *al.*, 2001]. The model is initialized with temperature and salinity fields that varied
301 meridionally as in *Xu et al.* [2012]. The initial NO₃ field is derived from fitting winter
302 data from main stem stations with a power function [Xu and Hood, 2006]. The remaining
303 biological variables are set to the following horizontally uniform values: [NH₄] = 0.1
304 mmole-N m⁻³; P = 6 mmole-N m⁻³; Z = 1 mmole-N m⁻³; D_S = 6.66 mmole-N m⁻³; D_L =
305 3.33 mmole-N m⁻³; [DON]_{SL} = 13 mmole-N m⁻³; [DON]_R = 23 mmole-N m⁻³, [Chl] = 15
306 mg-Chl m⁻³, [O₂] = 281.25 mmole-O₂ m⁻³ and ISS = 7 mg L⁻¹ All initial fields are
307 vertically uniform.

308 The model was first run starting with the above initial conditions from 1 January
309 2000 until 31 December 2005. The simulated distributions from 31 December 2005 were
310 then used to restart the model on 1 January 2000 and the model was run until 31
311 December 2005 again. In total, this six-year run was conducted five times to ensure the
312 model was spun up adequately, i.e, there was no clear linear trend for any physical or
313 biological variables and the fluctuations of each of the variables were nearly identical
314 between the fourth and fifth simulations. The last 5-years of this simulation was used for
315 analysis (2001-2005).

316 **3. Model Skill Assessment**

317 Quantitative model-data comparisons using multiple skill metrics [Jolliff *et al.*,
318 2009; Stow *et al.*, 2009] are critical, as they reveal the advantages and potential
319 limitations of a particular model, which must be carefully considered before using such a
320

321 model as a tool for scientific study or decision-making. Using the skill metrics described
322 in supporting information S2, the simulated physical fields (including temperature and
323 salinity) and biogeochemical fields (including NO_3 , NH_4 , DON, PON, chlorophyll and
324 oxygen) were compared with EPA Chesapeake Bay Program Water Quality Monitoring
325 Data.

326 The Chesapeake Bay Program has been routinely monitoring the main stem of the
327 Chesapeake Bay since June 1984. Specifically, throughout our analysis time period
328 (2001-2005) many water quality parameters, including various forms of nitrogen as well
329 as water temperature, salinity, and dissolved oxygen, were measured once each month
330 during the colder late fall/winter/spring months, and twice each month during the warmer
331 months. At each station (Fig. 1b), vertical profiles of water temperature, salinity and
332 dissolved oxygen were measured at approximately 1- to 2- m intervals through the water
333 column. Data on other variables such as NO_3 , NH_4 , DON, PON, and chlorophyll were
334 collected in the surface and bottom layers, and at depths representing upper (above
335 pycnocline) and lower (below pycnocline) layers in the deeper main-stem stations where
336 salinity stratification occurs.

337 In addition to comparing simulated fields with these in situ data, simulated
338 surface chlorophyll fields were also compared with satellite-derived surface chlorophyll
339 concentrations from the Sea-viewing Wide Field-of-view Sensor (SeaWiFS). For this
340 purpose, monthly SeaWiFS data for the Chesapeake Bay were processed at a spatial
341 resolution of 2 km using the OC4v6 chlorophyll algorithm.

342 **3.1 Evaluation of Hydrodynamic Fields**

343 Although the focus of this analysis is on the nitrogen budget of the Chesapeake
344 Bay, reasonable nutrient distributions cannot be obtained without an adequate simulation
345 of the observed hydrodynamic fields. Thus simulated temperature and salinity fields were
346 extensively compared to CBP observations.

347 **3.1.1 Temperature**

348 Seasonally averaged simulated temperature distributions are in very good
349 agreement with CBP observations throughout the water column (Fig. 3). Monthly depth-
350 averaged temperature in three Bay subareas, the upper, middle and lower Bay (Fig. 1),
351 show comparable magnitude and fluctuations in both model and observations (Fig. 4).
352 Although the temperature field shows significant temporal variability, increasing from
353 0°C to 30°C between winter and summer (Fig. 4), there is little horizontal or vertical
354 variability within any given season, with average temperatures being nearly uniform
355 throughout the water column and throughout the main stem of the Bay (Fig. 3). Model
356 skill statistics for temperature (presented in Table 1, and summarized in Taylor and target
357 diagrams (Fig. 5)), indicate that correlations between the simulated and observed
358 temperature fields are very high (> 0.99) and the normalized unbiased RMSD (≤ 0.2) and
359 Bias (≤ 0.1) are both very small. Both temporal and spatial Willmott skill is close to 1.0,
360 further demonstrating that the model has significant skill in reproducing the observed
361 temperature field.

362 **3.1.2 Salinity**

363 Stratification is typically dominated by the salinity signal in the Chesapeake Bay,
364 and thus it is critical for the model to accurately represent the salinity field. Seasonally

365 averaged simulated salinity distributions are in very good agreement with CBP
366 observations throughout the water column (Fig. 6), successfully capturing both the
367 horizontal and vertical gradients in salinity concentrations. In contrast to that of the
368 temperature field, the spatial variability of the salinity field is much stronger than that of
369 the temporal variability. Observed and simulated salinities vary from ≤ 5 PSU in the
370 upper Bay to ≥ 25 PSU in the lower Bay where seawater intrudes into the Bay mouth.
371 Specifically, over this time period the observed (simulated) averaged salinity \pm standard
372 deviation in the upper Bay is 3.5 ± 4.2 (4.1 ± 4.4), in the middle Bay is 15 ± 3.5 ($14 \pm$
373 3.8), and in the lower Bay is 22 ± 3.7 (22 ± 4.3). The simulated and observed salinity
374 distributions also show significant interannual variability (Fig. 7), which is strongly
375 influenced by the variable riverine inputs. For example, average salinity was particularly
376 low in 2004, which was an unusually wet year characterized by strong riverine inputs.
377 Although the temporal model skill for salinity is not quite as high as for temperature (Fig.
378 5, Table 1), correlations between modeled and observed salinity are greater than 0.7 and
379 Willmott skill is greater than 0.85.

380 **3.2 Evaluation of Biogeochemical Fields**

381 Simulated nitrogen (NO_3 , NH_4 , PON and DON), chlorophyll and oxygen fields
382 were also compared with CBP observations. A quantitative skill assessment analysis was
383 performed on both the temporally averaged distributions and the spatially averaged
384 distributions, in order to quantify how well the model captures both the spatial and the
385 temporal (monthly) variability. Finally, the simulated surface chlorophyll concentrations
386 were compared with those derived from SeaWIFS, in which case skill was assessed at
387 each pixel.

388 3.2.1 NO₃

389 The simulated NO₃ field successfully captures the horizontal gradient of the
390 observed CBP NO₃ + NO₂ field (Fig. 8a, b). Nitrate concentration is about 60 mmole-N
391 m⁻³ in the upper Bay throughout the water column, decreases rapidly to <15 mmole-N m⁻³
392 in the middle Bay, and is routinely lower than 5 mmole-N m⁻³ in the lower Bay. The
393 observed and simulated nitrate fields show little vertical gradient throughout most of the
394 Bay, with the exception of the transition zone between the upper and middle Bay (CBP
395 station CB3.2, CB3.3C and CB4.1C). The vertically integrated, simulated NO₂ + NO₃
396 field reproduces both the magnitude and seasonal cycle of the observations in the upper
397 Bay (Fig. 9a): the observed (simulated) values reach 1.3 ± 0.6 (1.5 ± 0.5) mole-N m⁻² in
398 January, gradually decrease to 0.6 ± 0.5 (0.6 ± 0.3) mole-N m⁻² in August, and increase to
399 1.1 ± 0.5 (1.4 ± 0.7) mole-N m⁻² again in December. In the middle and lower Bay, the
400 model has more difficulty reproducing the observed seasonal variability: the simulated
401 nitrate is in agreement with the observations for most of the year, but over-estimates the
402 observations in winter, though the observational variability is particularly large in these
403 winter months. As a result, Wilmott skill of NO₂ + NO₃ is higher in the upper Bay (0.84)
404 than in the middle (0.74) or lower Bay (0.34), since concentrations in the upper Bay are
405 primarily dependent on the riverine inputs and physical (advective/diffusive) processes
406 which are well prescribed in this modeling system. Overall, as was the case for salinity
407 and almost all biogeochemical variables, the model demonstrates a greater skill in
408 reproducing the observed spatial mean and variability along the main stem of the Bay,
409 than the interannual mean and monthly variability. Correlations between the simulated
410 and observed distributions are 0.98 (0.64) for the space (time) series. Similarly, the

411 spatial model skill for NO_3 was as high as 0.99, whereas the temporal model skill was
412 somewhat lower (0.77).

413 **3.2.2 NH_4**

414 Although the model reproduces the spatial variability of the ammonium field
415 relatively well, the magnitude is overestimated, particularly in the upper and middle Bay
416 (Fig. 8c, d). The depth of the strong vertical gradient of NH_4 apparent in the observations
417 (~10-15m) was considerably deeper than that of the simulated NH_4 fields (5-10m). The
418 bottom regeneration causing this vertical gradient may be overly strong in the model.
419 Close to the mouth of the estuary (CBP station CB7.3 and CB7.4), the model successfully
420 reproduces low ammonium concentrations throughout the water column. The model also
421 reproduces the observed pattern of higher NH_4 in the middle Bay compared to other
422 regions of the Bay (Fig. 9b, h, n), but the model somewhat underestimates the magnitude
423 of the seasonal cycle in this region, regenerating too much organic matter in the fall and
424 winter months in this region (Fig. 9h). The depth integrated annual average observed
425 (modeled) NH_4 concentrations in the upper Bay are 0.12 ± 0.13 (0.18 ± 0.12) moleN m^{-2} ,
426 in the middle Bay are 0.25 ± 0.3 (0.43 ± 0.33) moleN m^{-2} , and in the lower Bay are 0.068
427 ± 0.064 (0.074 ± 0.083) moleN m^{-2} , respectively. The quantitative skill of the simulated
428 ammonium distributions are summarized in the Taylor and target diagrams (Fig. 5). As is
429 the case for NO_3 , the model has more skill in repeating the observed spatial variability
430 than the temporal variability. Correlations between the simulated and observed
431 distributions are 0.94 (0.74) for the space (time) series. Overall, the spatial model skill
432 was 0.87, whereas the temporal model skill was again somewhat lower (0.65).

433 **3.2.3 PON**

434 The model reproduced the structure of the observed PON field throughout most of
435 the upper and middle Bay (stations CB2.1 to CB5.3), but overestimated PON in the lower
436 portions of the Bay (stations CB5.4 to CB7.4) (Fig. 7e, f). At the upper Bay stations, the
437 observed (modeled) PON concentration was as low as 15 ± 8 mmole-N m^{-3} (14 ± 10
438 mmole-N m^{-3}) throughout the water column. In the middle Bay, the observed (modeled)
439 PON was as high as 21 ± 9 mmole-N m^{-3} (16 ± 8 mmole-N m^{-3}) above 10 m, but as low
440 as 15 ± 6 mmole-N m^{-3} (12 ± 9 mmole-N m^{-3}) below 10 m. This structure resulted from
441 the fact that phytoplankton growth was not as light limited in the surface middle Bay
442 waters, as it was nearer the Susquehanna River, where high ISS and CDOM
443 concentrations significantly decreased phytoplankton growth rates. The annual cycle of
444 depth-integrated PON (Fig 9. c, i, o) illustrates that the PON in the middle Bay is
445 overestimated in the summer, primarily from May to September, when phytoplankton
446 growth is overestimated. In the upper Bay, observed PON shows a peak in March,
447 however this peak is associated with large interannual variability (0.72 ± 0.70 mole-N m^{-2})
448 ²) and the modeled concentrations are within this range (0.25 ± 0.11 mole-N m^{-2}).
449 Correlations between simulated and observed PON concentrations were 0.93 (0.25) for
450 spatial (time) series (Fig. 5). Overall PON spatial model skill (Table 1) was as high as
451 0.88, whereas temporal model skill was somewhat lower (0.52).

452 **3.2.4 DON**

453 As is the case for ammonium, observed DON concentrations are highest in the
454 middle Bay, and somewhat lower in the upper and lower Bay. The modeled DON
455 concentrations are generally in agreement with the mean observed DON concentrations,
456 but the model tends to overestimate DON in the upper Bay and at some stations near the

457 division between the middle and lower Bay (Fig. 8g, h). The mean observed (simulated)
458 DON concentration in the upper Bay is 21 ± 6 (17 ± 4) mmole-N m^{-3} ; in the middle Bay
459 is 22 ± 4 (20 ± 4) mmole-N m^{-3} ; and in the lower Bay is 19 ± 4 (14 ± 3) mmole-N m^{-3} .
460 The observed DON concentrations show only a slight seasonal signal, with higher
461 concentrations from October through January; this is not well represented in the
462 simulated distributions, which show relatively high concentrations from March to June in
463 both the middle and lower Bay (Fig. 9, d, j, p). Because the model reverses the observed
464 temporal DON pattern, the temporal correlation between modeled and observed DON is
465 negative (-0.17; Fig. 5) and the temporal model skill is low (0.38; Table 1); however, the
466 model has a high skill in reproducing the spatial variability (correlation = 0.98; spatial
467 model skill = 0.96).

468 **3.2.5 Dissolved Oxygen Field**

469 The model reproduces the observed oxygen distributions in the Bay very well. In
470 the upper and lower Bay, both simulated and observed oxygen concentrations are
471 consistently high throughout the water column, whereas in the middle Bay, both
472 simulated and observed oxygen concentrations show a strong vertical gradient (Fig. 8k,
473 l). The model also successfully reproduces the observed vertically integrated dissolved
474 oxygen seasonal cycle (Fig. 9f, l, and r), which closely follows the seasonal cycle of
475 temperature, largely due to the solubility effect of oxygen. Quantitatively, both spatial
476 and temporal model skill are high for dissolved oxygen, with correlations between the
477 simulated and observed fields reaching 0.98 in terms of both space and time (Fig. 5) and
478 overall spatial and temporal model skill both as high as 0.97.

479 **3.2.6 Chlorophyll**

480 The model reproduces the structure of the observed chlorophyll field throughout
481 most of the upper and lower Bay. However, in the middle Bay, the model is in agreement
482 with the observations above 10 m, but underestimates them in deeper waters (Fig. 8 i, j).
483 Not surprisingly, the annual cycle of chlorophyll (Fig. 8 e, k, q) shows a pattern similar to
484 that of PON in the upper and middle Bay for both model and observations, since a
485 significant component of PON is phytoplankton. As is the case for PON, the model
486 overestimates chlorophyll in the middle and upper Bay primarily from May to September
487 when phytoplankton growth is too high, and underestimates chlorophyll in the winter
488 when phytoplankton growth is too low. In addition, observed chlorophyll also shows a
489 peak in March in the upper Bay, however, this peak is associated with large interannual
490 variability ($0.35 \pm 0.43 \text{ g-Chl m}^{-2}$) and the modeled concentrations are within this range
491 ($0.11 \pm 0.07 \text{ g-Chl m}^{-2}$). Overall correlation between model and observations was 0.92
492 (0.33) for spatial (time) series (Fig. 5). Overall spatial model skill for chlorophyll was as
493 high as 0.94, whereas the temporal model skill was 0.49.

494 The averaged simulated surface chlorophyll fields were also compared with
495 SeaWiFS-derived chlorophyll concentrations (Fig. 10). The model successfully captures
496 the spatial along-Bay gradient of surface chlorophyll with an overestimation of the
497 satellite-derived estimates in the middle and lower Bay. The five-year mean surface
498 chlorophyll distributions show very low RMSD and high Wilmott skill in the northern
499 half of the Bay, but show some positive bias in the southern half of the Bay. The median
500 value of temporal model skill throughout the Bay is 0.49 (Fig. 10f). The five-year mean
501 vertically integrated primary production was also computed as $1321 \text{ mg-C m}^{-2} \text{ d}^{-1}$, which

502 is comparable to the mean net primary production ($1357 \text{ mg-C m}^{-2} \text{ d}^{-1}$) derived from
503 MODIS-Aqua [Son *et al.*, 2014].

504 **4. Results and Discussion**

505

506 **4.1 Mean nitrogen fluxes**

507

508 A mean nitrogen budget for the Chesapeake Bay covering the time period 2001-
509 2005 was computed from the simulated fields described above (Fig. 11). The average
510 total riverine nitrogen (inorganic + organic) entering the Chesapeake Bay as computed
511 from DLEM was $154 \times 10^9 \text{ g-N y}^{-1}$, with roughly 60% of this being present in the
512 inorganic form ($\text{NO}_3 + \text{NH}_4$). Burial removed about 30% of the riverine nitrogen entering
513 the Bay ($46 \pm 10 \times 10^9 \text{ g-N y}^{-1}$), with less than half of this occurring in the main stem
514 (Table 2). Together, water-column denitrification and sediment denitrification removed
515 roughly 20% of the riverine nitrogen entering the Bay ($34 \pm 10 \times 10^9 \text{ g-N y}^{-1}$; Fig. 11),
516 with more than half of this occurring in the main stem. The largest term representing loss
517 of total nitrogen was advective export to the coastal ocean. Although ocean export of
518 inorganic nitrogen was essentially negligible, the export of organic nitrogen was the
519 largest of the nitrogen loss terms ($91 \pm 36 \times 10^9 \text{ g-N y}^{-1}$). Together, the large amount of
520 inorganic nitrogen entering the Bay from the rivers coupled with the large amount of
521 organic nitrogen exiting the Bay through the Bay mouth is indicative of a system
522 characterized by a positive net ecosystem production ($\text{NEP} = 74 \pm 23 \times 10^9 \text{ g-N y}^{-1}$). This
523 is consistent with other studies, which have similarly reported that the Chesapeake Bay
524 acts as a net autotrophic estuary with production of organic nitrogen exceeding the loss of
525 organic nitrogen due to remineralization processes [Fisher *et al.*, 1988; Kemp *et al.*,
526 1997; 2005].

527 Our simulated nitrogen budget for 2001-2005 is surprisingly comparable to earlier
528 budgets derived from observations for both the whole Bay [*Boynton et al.*, 1995] and the
529 main stem [*Kemp et al.*, 1997], especially when considering that these estimates were
530 based on different time periods. The observationally based estimates were made using
531 data from 1975-1990, whereas the model was implemented for 2001-2005. Despite these
532 differing time periods of analysis, burial and denitrification rate estimates were very
533 similar, with the data derived estimates falling within the standard deviation of the
534 simulated estimates (Table 2) again for both the main stem [*Kemp et al.*, 1997] and the
535 Bay as a whole [*Boynton et al.*, 1995.] The advective ocean export fluxes calculated
536 using the two different methods were also surprisingly comparable, again especially
537 when considering the significant interannual variability (standard deviations) in the
538 simulated fluxes (Table 2). Finally, the net ecosystem production derived from our
539 ROMS-ECB simulation was calculated to be 5% - 9% of total annual primary production,
540 again in good agreement with the 8% reported by *Kemp et al.* [1997].

541 **4.2 Interannual variability of annual mean nitrogen fluxes**

542 The simulated nitrogen fluxes in the Bay vary considerably on interannual time
543 scales, as quantified by the high standard deviations associated with the individual annual
544 mean fluxes discussed above (Fig. 11). Although some interannual variability exists in
545 the wind, precipitation and radiative forcing, the primary source of this variability is river
546 discharge. For the five years analyzed, the DLEM freshwater river discharge varied by
547 more than a factor of two, from a mean of roughly $50 \text{ km}^3 \text{ y}^{-1}$ over the two lowest flow
548 years (2001-2002) to a mean of nearly $128 \text{ km}^3 \text{ y}^{-1}$ over the two highest flow years (2003-
549 2004; Fig. 12a.) This strong interannual variability in freshwater discharge estimated by

550 DLEM [Yang *et al.*, 2014a] closely matches (Table 3) that estimated by the regulatory
551 EPA Chesapeake Bay Watershed Model (CBP WM), which has been well tuned to
552 observations from USGS gauging stations [Shenk and Linker, 2013]: 2001-2002 = 56
553 km³ y⁻¹ and 2003-2004 = 122 km³ y⁻¹ (Shenk and Hinson, pers. comm.)

554 The strong interannual variability in freshwater discharge entering the Bay leads
555 to a similarly strong interannual variability in DIN and TON inputs into the Bay (Fig.
556 12b). Specifically, riverine inputs of TON for the high flow years of 2003-2004 (DLEM:
557 81 x10⁹ kg y⁻¹; CBP WM: 75 x10⁹ kg y⁻¹) are more than twice those of 2001-2002
558 (DLEM: 38 x10⁹ kg y⁻¹; CBP WM: 32 x10⁹ kg y⁻¹), with once again a similar magnitude
559 for both the DLEM and CBP WM estimates (Table 3). Both the DLEM and CBP WM
560 also indicate that the interannual variability of riverine DIN inputs is strong as well,
561 though this interannual variability estimated by DLEM is somewhat stronger than that of
562 the CBP WM (Table 3). Between 2001-2002 and 2003-2004, DLEM estimates a factor of
563 ~2.5 increase in riverine DIN input, while the CBP WM estimates an increase by a factor
564 of closer to 1.5 (Fig 12b).

565 The impact of interannual variability of nitrogen inputs on nitrogen fluxes within
566 the Bay is strong. Although the magnitude of NEP, denitrification, burial and ocean
567 export fluxes were higher in high flow years and lower in low flow years, the magnitude
568 of this interannual variability does not vary linearly with freshwater discharge. For
569 example, DLEM estimated that the freshwater discharge increased 160% from the two
570 lowest to the two highest flow years and was associated with a similarly large (150%)
571 increase in riverine input of DIN; however, the resulting variability in the estuarine
572 biogeochemical fluxes was considerably smaller. Burial, and denitrification increased by

573 only about 50% ($19 \times 10^9 \text{ kg y}^{-1}$) and 70% ($18 \times 10^9 \text{ kg y}^{-1}$) respectively, between these
574 pairs of years.

575 Interannually varying riverine inputs also impact the advective export of DIN and
576 TON to the coastal ocean. The increase in TON export for the high flow vs. low flow
577 years was even greater in magnitude ($69 \times 10^9 \text{ kg y}^{-1}$) than the increase in TON riverine
578 input ($43 \times 10^9 \text{ kg y}^{-1}$). This result, i.e. the fact that the export of TON increased more than
579 the input of TON, can be explained by examining the inorganic nitrogen fluxes.
580 Specifically, the increase in DIN export for the high flow vs. low flow years was
581 considerably smaller in magnitude ($14 \times 10^9 \text{ kg y}^{-1}$) than the increase in DIN riverine input
582 ($86 \times 10^9 \text{ kg y}^{-1}$). The remaining excess DIN entering the estuary that was not exported to
583 the coastal ocean was either denitrified, or transformed into organic nitrogen prior to
584 export to the continental shelf.

585 **4.3 Comparison of simulated fluxes with those from a continental shelf**

586 **biogeochemical model**

587 The Chesapeake Bay nitrogen fluxes computed using the ROMS-ECB estuarine
588 model are significantly different (Table 3) from those computed using a regional
589 biogeochemical shelf model configured for the mid-Atlantic Bight [*Druon et al.*, 2010;
590 *Hofmann et al.*, 2011; *Xiao and Friedrichs*, 2014a,b; *Friedrichs et al.*, in prep for this
591 issue]. The version of the regional shelf model used here for comparison (Table 4) did not
592 include the estuarine specific processes developed for ROMS-ECB (Section 2.2) such as
593 light attenuation due to inorganic suspended solids, estuarine specific phytoplankton
594 growth rates, water column denitrification and oxygen limitation of remineralization.
595 Although the riverine fluxes to the Chesapeake Bay are generally comparable for the two

596 models over the various years examined, the burial and denitrification fluxes computed
597 from the estuarine model removed nearly an order of magnitude more nitrogen from the
598 Bay than did the coastal model (Table 4). In addition, although the total ocean export of
599 nitrogen was similar for the two models, the estuarine model exported almost entirely
600 TON and very little DIN. In contrast, the regional shelf model exported nearly equal
601 amounts of TON and DIN. The critical nitrogen transformations that occur within the
602 estuary were not successfully represented in the regional model, and thus this model
603 overestimated the transport of riverine DIN to the coastal ocean.

604 The above results demonstrate the importance of resolving estuarine-specific
605 processes in larger scale regional models that include estuarine domains. This is
606 specifically critical for regions receiving considerable amounts of inorganic nutrients and
607 organic matter from estuaries, such as the Mid-Atlantic Bight [*Nixon, 1987*] and the
608 Louisiana Shelf [*Feng et al., 2012; 2014*]. In these regions it will likely be necessary and
609 will certainly be most efficient to have relatively high-resolution models specifically
610 developed for estuaries nested inside potentially coarser resolution regional shelf models.
611 Fortunately, many of the critical estuarine biogeochemical formulations in ROMS-ECB
612 are active only in regions of low dissolved oxygen concentrations and high inorganic
613 suspended solids. Since these conditions are not generally present in the mid-Atlantic
614 Bight shelf adjacent to the Chesapeake Bay, the ECB model is likely to successfully
615 reproduce biogeochemical processes on the outer shelf as well as in the Chesapeake Bay.
616 Research devoted to testing this hypothesis is currently underway.

617 **5. Summary**

618 In this study the interannual variability associated with physical and
619 biogeochemical nitrogen fluxes in the Chesapeake Bay has been quantified by means of
620 an estuarine-biogeochemical model (ECB) coupled to a three-dimensional hydrodynamic
621 model (ROMS) and forced by a terrestrial ecosystem model (DLEM). The estuarine
622 model was based on previous mid-Atlantic Bight models [*Druon et al.*, 2010; *Hofmann et*
623 *al.*, 2008; 2011], but was modified to include key estuarine processes including light
624 attenuation due to inorganic suspended solids, estuarine specific phytoplankton growth
625 rates, water column denitrification and oxygen limitation of remineralization. The
626 ROMS-ECB-DLEM implementation described here shows significant skill in
627 reproducing the variability of both physical and biogeochemical fields of the Bay when
628 evaluating with in-situ and satellite-derived data for a contemporary period (2001-2005).
629 In addition, the nitrogen fluxes computed with this modeling system closely match mean
630 fluxes derived from historical Chesapeake Bay observations, which is particularly
631 surprising given the strong interannual variability associated with these fluxes. Although
632 a number of 3D coupled estuarine models have been previously implemented in the
633 Chesapeake Bay [*Cerco*, 2002; *Li et al.*, 2009; *Testa et al.*, 2014; *Xu and Hood* 2006;
634 *Scully*, 2010; 2013], these previous efforts have been limited to examining one or two
635 specific aspects of estuarine biogeochemistry associated with nitrogen cycling, such as
636 phytoplankton biomass, dissolved inorganic nutrients, or dissolved oxygen
637 concentrations. To our knowledge, this is the first time both physical and biogeochemical
638 components of the complete Chesapeake Bay nitrogen cycle have been investigated using
639 a coupled hydrodynamic-biogeochemical model.

640 The continuous 5-year period selected for analysis incorporated very different
641 hydrological conditions: dry (2001 and 2002), wet (2003 and 2004) and intermediate
642 (2005). The comparison of nitrogen fluxes obtained for these different hydrological
643 conditions shows that although the magnitude of total nitrogen input from rivers is
644 approximately proportional to river freshwater discharge, the estuarine biogeochemical
645 fluxes, i.e. burial, denitrification and net ecosystem production, are not. An increase of
646 total nitrogen into the Bay of $100 \times 10^9 \text{ kg y}^{-1}$ (including $40 \times 10^9 \text{ kg y}^{-1}$ of TON and 60×10^9
647 kg y^{-1} of DIN), which is similar to the difference between the high flow year of 2004 and
648 the low flow year of 2001, results in relatively small increases in denitrification, burial
649 and DIN export to the coastal ocean ($10\text{-}15 \times 10^9 \text{ kg y}^{-1}$). In contrast, such an increase in
650 total nitrogen into the Bay results in nearly a $50\text{-}60 \times 10^9 \text{ kg y}^{-1}$ input of TON to the
651 coastal ocean. Thus increased DIN input to the Bay is not exported directly as DIN to the
652 coastal ocean, but rather is primarily denitrified, or converted to TON before advected
653 out of the Bay.

654 Three-dimensional (3D) coupled hydrodynamic-biogeochemical models have
655 been widely used in recent years for the study of marine biogeochemical cycling within
656 ocean margins, and provide a useful tool for examining the transformation of nutrients in
657 coastal regions [*Banas et al.*, 2009; *Druon et al.*, 2010; *Feng et al.*, 2014; *Fennel et al.*,
658 2006; 2011; *Friedland et al.*, 2012; *Wakelin et al.*, 2012; *Xue et al.*, 2013]. However
659 estuaries, which play an important role in global nutrient cycling, are often poorly
660 represented in these types of models. Regional and basin-scale models typically either
661 export riverine nutrients to coastal waters directly omitting the estuaries altogether, or
662 include estuarine regions but apply biogeochemical models derived for continental

663 shelves to the estuarine domains (e.g., *Fennel et al.* [2006], *Druon et al.* [2010], *Hofmann*
664 *et al.*, [2008; 2011]). Here nitrogen exported from the Chesapeake Bay computed from
665 the estuarine-specific ECB model was compared with a model developed for the U.S.
666 eastern continental shelf. The significant resulting differences in DIN export (49 ± 10
667 $\times 10^9$ gN yr⁻¹ for the coastal model vs. $8 \pm 8 \times 10^9$ gN yr⁻¹ for the estuarine model)
668 highlight the importance of carefully resolving estuarine physical and biogeochemical
669 processes in regional and basin scale models.

670 Although the ROMS-ECB-DLEM simulations documented here closely
671 replicated nitrogen fluxes derived from observations in the Chesapeake Bay, future
672 efforts will be devoted to further improving the Chesapeake Bay model implementation.
673 First, atmospheric nitrogen deposition, estimated to contribute 12% of the total nitrogen
674 input to the Bay, and commercial fisheries harvest, estimated to only contribute ~3%
675 error [*Boynton et al.*, 1995] have not been included in our budget analysis. These terms
676 will be estimated in future analyses. Secondly, our NPZD-structured model includes a
677 very simplified ecosystem, with only one type of phytoplankton and zooplankton,
678 whereas in reality multiple distinct phytoplankton species are present in the Bay
679 [*Marshall and Nesius*, 1996]. Although efforts are currently underway to expand the
680 model to include multiple phytoplankton and zooplankton components [*Xiao and*
681 *Friedrichs*, 2014a; 2014b], this will still represent a dramatic over-simplification of the
682 Chesapeake Bay ecosystem, which includes other producers such as submerged plants
683 and benthic algae. These primary producers do contribute to nitrogen fluxes, however it
684 is likely that our simulated nitrogen budgets are still quite robust, as the primary
685 producers within the main stem are dominated by phytoplankton. Possible further

686 improvements to ROMS-ECB include the incorporation of other nutrient limitation
687 effects such as phosphate and silicate [*Fisher et al.*, 1992] and refining our representation
688 of pelagic-benthic coupling processes. Finally, although ROMS-ECB includes a full
689 carbon cycle (not described here), many of the carbon formulations are more similar to
690 those described in the continental shelf models of *Fennel et al.* [2008] and *Druon et al.*
691 [2010]. These formulations and parameterizations need to be updated so that they are
692 more representative of estuarine systems.

693 A significant difference between previous Chesapeake Bay model
694 implementations and the modeling effort described here, is that our river forcing is
695 provided by a process based terrestrial ecosystem model. An advantage of linking our
696 estuarine biogeochemistry model directly to such a terrestrial ecosystem model is that the
697 impacts on estuarine nutrient cycling processes of past and future changes in climate,
698 land use and land cover can be examined. Such past and future scenario simulations are
699 currently being conducted and will be described in follow-up studies. As a result, our
700 linked modeling system will likely not only benefit future estuarine scientific studies, but
701 also support management applications and future high stakes decision-making.

702 **Acknowledgments**

703 This work was supported by the NASA Interdisciplinary Science Program
704 (NNX11AD47G). The authors are grateful to the NASA U.S. Eastern Continental Shelf
705 Carbon Cycling (USECoS) team for their useful comments. We thank Jeremy Werdell
706 for providing the high-resolution SeaWiFS chlorophyll level3 data, and Kyle Hinson and
707 Gary Shenk for providing us with Phase 5.3.2 output from the Chesapeake Bay Program
708 Watershed Model. This is VIMS contribution # xxxx.

709 **References**

710 Banas, N. S., E. J. Lessard, R. M. Kudela, P. MacCready, T. D. Peterson, B. M. Hickey,
711 and E. Frame (2009), Planktonic growth and grazing in the Columbia River plume region:
712 A biophysical model study, *J. Geophys. Res.-Oceans*, *114*, C00B06,
713 doi:10.1029/2008JC004993.

714

715 Bauer, J. E., W.-J. Cai, P. A. Raymond, B. T. S., C. S. Hopkinson, and P. A. G. Regnier
716 (2013), The changing carbon cycle of the coastal ocean, *Nature*, *504*, 61-70, doi:
717 10.1038/nature12857.

718

719 Bever, A. J., M. A. M. Friedrichs, C. T. Friedrichs, M. E. Scully, L. W. J. Lanerolle
720 (2013),
721 Combining observations and numerical model results to improve estimates of hypoxic
722 volume within the Chesapeake Bay, USA. *J. Geophys. Res.: Oceans*, *118*, 4924-4944,
723 <http://dx.doi.org/doi:10.1002/jgrc.20331>.

724

725 Bianchi, T. S., and J. E. Bauer (2011), Particulate Organic Carbon Cycling and
726 Transformation, in *Treatise on Estuarine and Coastal Science*, edited by Wolanski E. and
727 McLusky D.S., pp. 69-117, Waltham: Academic Press.

728

729 Boynton, W. R., J. H. Garber, R. Summers, and W. M. Kemp (1995), Inputs,
730 transformations, and transport of nitrogen and phosphorus in Chesapeake Bay and
731 selected tributaries, *Estuaries*, *18*, 285-314, doi:10.2307/1352640.

732

733 Bronk, D. A., P. M. Gilbert, T. C. Malone, S. Banahan, and E. Sahlsten (1998), Inorganic
734 and organic nitrogen cycling in Chesapeake Bay: autotrophic versus heterotrophic
735 processes and relationships to carbon flux, *Aquat Microb Ecol*, 15, 177-189.

736

737 Brown, C. W., R. R. Hood, W. Long, J. Jacobs, D. L. Ramers, C. Wazniak, J. D. Wiggert,
738 R. Wood, and J. Xu (2013), Ecological forecasting in Chesapeake Bay: Using a
739 mechanistic–empirical modeling approach, *J. Mar. Syst.*, 125, 113-125,
740 doi:10.1016/j.jmarsys.2012.12.007.

741

742 Cai, W.-J. (2011), Estuarine and Coastal Ocean Carbon Paradox: CO₂ Sinks or Sites of
743 Terrestrial Carbon Incineration?, *Annu. Rev. Mar. Sci.*, 3, 123-145, doi:10.1146/annurev-
744 marine-120709-142723.

745

746 Canuel, E. A., S. S. Cammer, H. A. McIntosh, and R. P. Christina (2012), Climate
747 Change Impacts on the Organic Carbon Cycle at the Land-Ocean Interface, *Annu. Rev.*
748 *Earth Planet. Sci.*, 40, 685–711, doi:10.1146/annurev-earth-042711-105511.

749

750 Cerco, C. F. (2002), Phytoplankton Kinetics in the Chesapeake Bay Eutrophication
751 Model, *Water Quality and Ecosystem Modeling*, 1, 5-49.

752

753 Chapman, D. C. (1985), Numerical Treatment of Cross-Shelf Open Boundaries in a
754 Barotropic Coastal Ocean Model, *J. Phys. Oceanogr.*, 15, 1060-1075, doi:10.1175/1520-
755 0485(1985)015<1060:ntocso>2.0.co;2.
756

757 Curtin, P. D., G. S. Brush, and G. W. Fisher (2001), Discovering the Chesapeake: the
758 history of an ecosystem, Johns Hopkins University Press, Baltimore, MD.
759

760 Druon, J. N., A. Mannino, S. Signorini, C. McClain, M. Friedrichs, J. Wilkin, and K.
761 Fennel (2010), Modeling the dynamics and export of dissolved organic matter in the
762 Northeastern U.S. continental shelf, *Estuar. Coast. Shelf. S.*, 88, 488-507,
763 doi:10.1016/j.ecss.2010.05.010.
764

765 U.S. EPA (1982). Chesapeake Bay Program Technical Studies: A Synthesis. U.S.
766 Environmental Protection Agency, Washington, DC.
767

768 Eppley, R. W. (1972), Temperature and phytoplankton growth in the sea, *Fish. Bull.*, 70,
769 1063-1085.
770

771 Feng, Y., K. Fennel, G. A. Jackson, S. F. DiMarco, R. D. Hetland (2014), A model study
772 of the response of hypoxia to upwelling-favorable wind on the northern Gulf of Mexico
773 shelf, *J. Marine Syst.*, 131, 63-73, doi: 10.1016/j.jmarsys.2013.11.009
774

775 Feng, Y., S. F. DiMarco, and G. A. Jackson (2012), Relative role of wind forcing and
776 riverine nutrient input on the extent of hypoxia in the northern Gulf of Mexico, *Geophys.*
777 *Res. Lett.*, 39, L09601, doi:10.1029/2012GL051192.

778

779 Fennel, K., R. Hetland, and Y. Feng and S. F. DiMarco (2011), A coupled physical-
780 biological model of the northern Gulf of Mexico shelf: Model description, validation and
781 analysis of phytoplankton variability. *Biogeosciences* 8, 1881-1899, doi:10.5194/bg-8-
782 1881-201.

783

784 Fennel, K., J. Hu, A. Laurent, M. Marta-Almeida, and R. Hetland (2013), Sensitivity of
785 hypoxia predictions for the northern Gulf of Mexico to sediment oxygen consumption
786 and model nesting, *J. Geophys. Res. Oceans*, 118, doi:10.1002/jgrc.20077.

787

788 Fennel, K., J. Wilkin, J. Levin, J. Moisan, J. O'Reilly, and D. Haidvogel (2006), Nitrogen
789 cycling in the Mid Atlantic Bight and implications for the North Atlantic nitrogen budget:
790 Results from a three-dimensional model. , *Global Biogeochemical Cy.*, 20, GB3007,
791 doi:10.1029/2005GB002456.

792

793 Fennel, K., J. Wilkin, M. Previdi, and R. Najjar (2008), Denitrification effects on air-sea
794 CO₂ flux in the coastal ocean: Simulations for the northwest North Atlantic, *Geophys.*
795 *Res. Lett.*, 35, L24608, doi:10.1029/2008gl036147.

796

797 Fisher, T. R., J. Harding, L. W., D. W. Stanley, and L. G. Ward (1988), Phytoplankton,
798 Nutrients, and Turbidity in the Chesapeake, Delaware and Hudson Estuaries, *Estuar.*
799 *Coast. Shelf. S.*, 27, 61-93, doi:10.1016/0272-7714(88)90032-7
800
801 Fisher, T. R., E. R. Peele, J. W. Ammerman, and J. Harding, L. W. (1992), Nutrient
802 limitation of phytoplankton in Chesapeake Bay, *Mar. Eco-Pro. Ser.*, 82, 51-63,
803 doi:10.3354/meps082051.
804
805 Flather, R. A. (1976), A tidal model of the northwest European continental shelf, *Mem.*
806 *Soc. R. Sci. Liege*, 10, 141-164.
807
808 Flemer, D.A., G.B. Mackiernan, W. Nehlsen, V.K. Tippie, R.B. Biggs, D. Blaylock, N.H.
809 Burger, L.C. Davidson, D. Haberman, K.S. Price, and J.L. Taft (1983), Chesapeake Bay:
810 A profile of environmental change. U.S. Environmental Protection Agency, Chesapeake
811 Bay Program, Annapolis, Maryland.
812
813 Friedland, R., T. Neumann, and G. Schernewski (2012), Climate change and the Baltic
814 Sea action plan: Model simulations on the future of the western Baltic Sea, *J. Mar. Syst.*,
815 105–108, 175-186, doi:10.1016/j.jmarsys.2012.08.002.
816
817 Friedrichs, M. A. M., R. R. Hood, and J. D. Wiggert (2006), Ecosystem model
818 complexity versus physical forcing, quantification of their relative impact with

819 assimilated Arabian Sea data, *Deep-Sea Res. II*, 53, 576-600, doi:
820 10.1016/j.dsr2.2006.01.026
821
822 Garcia, H., and L. Gordon (1992), Solubility of oxygen at different temperature and
823 salinity, *Limnol. Oceanogr.*, 37, 1307–1312.
824
825 Gattuso, J.-P., M. Frankignoulle, and R. Wollast (1998), Carbon and carbonate
826 metabolism in coastal aquatic ecosystems, *Annu. Rev. Ecol. Syst.*, 29, 405–434,
827 doi:10.1146/annurev.ecolsys.29.1.405.
828
829 Glibert, P. M., C. Garside, J. A. Fuhrman, and M. R. Roman (1991), Time-dependent
830 coupling of inorganic and organic nitrogen uptake and regeneration in the plume of the
831 Chesapeake Bay estuary and its regulation by large heterotrophs, *Limnol. Oceanogr.*,
832 36(5), 895-909.
833
834 Hagy, J. D., W. R. Boynton, C. W. Keefe, and K. V. Wood (2004), Hypoxia in
835 Chesapeake Bay, 1950-2001 Long-term Change in Relation to Nutrient Loading and
836 River Flow, *Estuaries*, 27(4), 634-658.
837
838 Hofmann, E.E., J.-N. Druon, K. Fennel, M. Friedrichs, D. Haidvogel, C. Lee, A.
839 Mannino, R. Najjar, J. O'Reilly, D. Pollard, M. Previdi, S. Seitzinger, J. Siewert, S.
840 Signorini, and J. Wilkin (2008), Eastern U.S. continental shelf carbon budget: integrating
841 models, data assimilation, and analysis. *Oceanography*, 21(1), 86-104.

842

843 Hofmann, E. E., B. Cahill, K. Fennel, M.A.M. Friedrichs, K. Hyde, C. Lee, A. Mannino,
844 R.G.

845 Najjar, J.E. O'Reilly, J. Wilkin, J. Xue (2011), Modeling the dynamics of continental
846 shelf carbon, *Annu. Rev. Mar. Sci.*, 3, 93-122, doi:10.1146/annurev-marine-120709-
847 142740.

848

849 Hood, R., E. Laws, K. Moore, R. Armstrong, N. Bates, C. Carlson, F. Chai, S. Doney, P.
850 Falkowski, D. Feely, M.A.M. Friedrichs, M. Landry, R. Letelier, D. Nelson, T.
851 Richardson, B. Salihoglu, J. Wiggert, and M. Schartau (2006), Functional group
852 modeling: progress, challenges and prospects. *Deep-Sea Research II*, 53, 459-512.

853

854 Hopkinson, C. S., and E. M. Smith (2005), Estuarine respiration an overview of benthic,
855 pelagic, and whole system respiration, in *Respiration in Aquatic Ecosystems*, edited by P.
856 A. del Giorgio and P. J. B. Williams, Oxford Univ. Press, Oxford, U. K.,
857 doi:10.1093/acprof:oso/9780198527084.003.0008.

858

859 Horrigan, S. G., J. P. Montoya, J. L. Nevins, and J. J. McCarthy (1990), Natural isotopic
860 composition of dissolved inorganic nitrogen in the Chesapeake Bay, *Estuar Coast Shelf*
861 *Sci.*, 30(4), 393-410, doi:0.1016/0272-7714(90)90005-C.

862

863 Jolliff, J. K., J. C. Kindle, I. Shulman, B. Penta, M. A. M. Friedrichs, R. Helber, and R. A.
864 Arnone (2009), Summary diagrams for coupled hydrodynamic-ecosystem model skill
865 assessment, *J. Mar. Syst.*, 76, 64-82, doi:10.1016/J.Jmarsys.2008.05.014.
866

867 Kantha, L. H., and C. A. Clayson (1994), An improved mixed layer model for
868 geophysical applications, *J. Geophys. Res.- Oceans*, 99, 25235-25266,
869 doi:10.1029/94jc02257.
870

871 Kemp, W. M. (2005), Eutrophication of Chesapeake Bay: historical trends and ecological
872 interactions, *Mar. Eco-Pro. Ser.*, 303, 1-29, doi:10.3354/meps303001.
873

874 Kemp, W. M., and W. R. Boynton (1984), Spatial and temporal coupling of nutrient
875 inputs to estuarine primary production: the role of particulate transport and
876 decomposition, *B. Mar. Sci.*, 35, 522-535.
877

878 Kemp, W. M. (2005), Eutrophication of Chesapeake Bay: historical trends and ecological
879 interactions, *Mar. Eco-Pro. Ser.*, 303, 1-29, doi:10.3354/meps303001.
880

881 Kemp, W. M., E. M. Smith, M. M. Marvin-DiPasquale, and W. R. Boynton (1997),
882 Organic carbon balance and net ecosystem metabolism in Chesapeake Bay, *Mar. Eco-*
883 *Pro. Ser.*, 150, 229-248.
884

885 King, G.M., 2005. Ecophysiology of microbial respiration. In: P.A. Del Giorgio and
886 P.J.I.B. Williams (Editors), *Respiration in Aquatic Ecosystems*. Oxford University Press,
887 New York, pp. 18–35.
888

889 Li, M., L. Zhong, and J. Harding, L. W. (2009), Sensitivity of plankton biomass and
890 productivity to variations in physical forcing and biological parameters in Chesapeake
891 Bay, *J. Mar. Res.*, *67*, 667-700, doi: 10.1357/00222400979121887.
892

893 Liu, M., H. Tian, Q. Yang, J. Yang, X. Song, S. E. Lohrenz, and W.-J. Cai (2013), Long-
894 term trends in evapotranspiration and runoff over the drainage basins of the Gulf of
895 Mexico during 1901-2008, *Water Resour. Res.*, *49*, 1988 - 2012, doi:10.1002/wrcr.20180.
896

897 MacCready, P., and W. R. Geyer (2010), Advances in estuarine physics, *Annu. Rev. Mar.*
898 *Sci.*, *2*, 35-58, doi:10.1146/annurev-marine-120308-081015.
899

900 Marchesiello, P., J. C. McWilliams, and A. F. Shchepetkin (2001), Open boundary
901 conditions for long-term integration of regional oceanic models, *Ocean Modelling*, *3*, 1-
902 20. doi: 10.1016/S1463-5003(00)00013-5.
903

904 Marshall, H. G., and K. K. Nesius (1996), Phytoplankton composition in relation to
905 primary production in Chesapeake Bay, *Mar. Biol.*, *125*, 611-617,
906 doi:10.1007/BF00353272.
907

908 Meybeck, M. (1998), Man and river interface: multiple impacts on water and particulates
909 chemistry illustrated in the Seine river basin., *Hydrobiol*, 373/374, 1-20, doi:
910 10.1023/A:1017067506832.

911

912 Nixon, S. W. (1987), Chesapeake Bay nutrient budgets: a reassessment, *Biogeochemistry*,
913 4, 77-90.

914

915 Nixon, S. W., et al. (1996), The fate of nitrogen and phosphorus at the land-sea margin of
916 the North Atlantic Ocean, in *Nitrogen Cycling in the North Atlantic Ocean and its*
917 *Watersheds*, edited by R. Howarth, pp. 141-180, Springer Netherlands.

918

919 Oguz, T. (2002), Role of physical processes controlling oxycline and suboxic layer
920 structures in the Black Sea, *Global Biogeochemical Cy.*, 16, 1019,
921 doi:10.1029/2001GB001465.

922

923 Resplandy, L. et al., (2012), Controlling factors of the oxygen balance in the Arabian
924 Sea's OMZ. *Biogeosci.*, 9: 5095-5109: 10.5194/bg-9-5095-2012.

925

926 Richards, F., (1965), Anoxic basins and fjords. In: J.P. Ripley and G. Skirrow (Editors),
927 *Chemical Oceanography*, pp. 611-643.

928

929 Scully, M. E. (2010), Wind modulation of dissolved oxygen in Chesapeake Bay, *Estuar.*
930 *Coast*, 33, 1164-1175, doi:10.1007/s12237-010-9319-9.

931 Scully, M. E. (2013), Physical controls on hypoxia in Chesapeake Bay: A numerical
932 modeling study, *J. Geophys. Res.- Oceans*, 118, 1-18, doi:10.1002/jgrc.20138, 2013.
933

934 Shchepetkin, A. F., and J. C. McWilliams (2005), The regional oceanic modeling system
935 (ROMS): a split-explicit, free-surface, topography-following-coordinate oceanic model,
936 *Ocean Modelling*, 9, 347-404, doi:10.1016/J.Ocemod.2004.08.002.
937

938 Shchepetkin, A. F., and J. C. McWilliams (2009), Correction and commentary for
939 “Ocean forecasting in terrain-following coordinates: Formulation and skill assessment of
940 the regional ocean modeling system” by Haidvogel et al., *J. Comp. Phys.* 227, pp. 3595–
941 3624, *J. Comput Phys.*, 228, 8985-9000, doi:10.1016/j.jcp.2009.09.002.
942

943 Sheng, Y. P. (1986), A three-dimensional mathematical model of coastal, estuarine and
944 lake currents using a boundary fitted grid, Rep. No. 585, ARAR Group of Titan Systems,
945 Princeton, N. J.
946

947 Shenk, G.W. and L.C. Linker (2013), Development and application of the 2010
948 Chesapeake Bay watershed total maximum daily load model. *JAWRA*, 49:1042-1056.
949

950 Smith, S. V., and J. T. Hollibaugh (1993), Coastal metabolism and the oceanic organic
951 carbon balance, *Rev. Geophys*, 3, 75-89, doi:10.1029/92RG02584.
952

953 Smullen, J. T., J. Taft, and J. Macknis (1982), Nutrient and sediment loads to the tidal
954 Chesapeake Bay system, in Chesapeake Bay Program Technical Studies: a Synthesis,
955 edited by E. G. Macalaster, D. A. Barker and M. Kasper, pp. 147-262, U. S.
956 Environmental Protection Agency, Washington, D. C.

957

958 Son, S., M. Wang, and L. W. H. Jr. (2014), Satellite-measured net primary production in
959 the Chesapeake Bay, *Remote Sens. Environ.*, 144(25), 109-119,
960 doi:10.1016/j.rse.2014.01.018.

961

962 Stow, C. A., J. Jolliff, D. J. McGillicuddy, S. C. Doney, J. I. Allen, M. A. M. Friedrichs,
963 K. A. Rose, and P. Wallhead (2009), Skill assessment for coupled biological/physical
964 models of marine systems, *J. Mar. Syst.*, 76, 4-15, doi: 10.1016/J.Jmarsys.2008.03.011.

965

966 Tao, B., H. Tian, Q. Yang, S. Pan, W. Ren, B. Zhang, M.A.M. Friedrichs, R. Najjar, R.
967 (2014), Projected increase of river discharge to the U.S. East Coast forced by climatic
968 and anthropogenic scenarios during the 21st century. To be submitted to *J. of Geophys.*
969 *Res – Biogeosciences*.

970

971 Taylor, K. E. (2001), Summarizing multiple aspects of model performance in a single
972 diagram, *J. Geophys. Res.*, 106(D7), 7183–7192, doi:10.1029/2000JD900719.

973

974 Testa, J. M., Y. Li, Y. J. Lee, M. Li, D. C. Brady, D. M. D. Toro, W. M. Kemp, and J. J.
975 Fitzpatrick (2014), Quantifying the effects of nutrient loading on dissolved O₂ cycling

976 and hypoxia in Chesapeake Bay using a coupled hydrodynamic–biogeochemical model, *J.*
977 *Mar. Syst.*, 139, 139-158, doi:10.1016/j.jmarsys.2014.05.018.

978

979 Tian, H., G. Chen, M. Liu, C. Zhang, G. Sun, C. Lu, X. Xu, W. Ren, S. Pan and A.
980 Chappelka (2010), Model estimates of ecosystem net primary productivity,
981 evapotranspiration, and water use efficiency in the southern United States during 1895-
982 2007, *Forest Ecol. and Manag.* 259: 1311-1327.

983

984 Tian, H., G. Chen, C. Lu, X. Xu, D. J. Hayes, W. Ren, S. Pan, D. N. Huntzinger, and S. C.
985 Wofsy (2014), North American terrestrial CO₂ uptake largely offset by CH₄ and N₂O
986 emissions: toward a full accounting of the greenhouse gas budget, *Climatic Change*,
987 doi:10.1007/s10584-014-1072-9.

988

989 Wakelin, S. L., J. T. Holt, J. C. Blackford, J. I. Allen, M. Butenschön, and Y. Artioli
990 (2012), Modeling the carbon fluxes of the northwest European continental shelf:
991 Validation and budgets, *J. Geophys. Res.-Oceans*, 117, C05020,
992 doi:10.1029/2011jc007402.

993

994 Walsh, J. J. (1988), *On the Nature of Continental Shelves*, 520 pp., New York: Academic.

995

996 Wanninkhof, R. (1992), Relationship between wind speed and gas exchange, *J. Geophys.*
997 *Res.*, 97, 7373–7382.

998

999 Wang, Z., D. B. Haidvogel, D. Bushek, S. E. Ford, E. E. Hofmann, E. N. Powell, and J.
1000 Wilkin (2012), Circulation and water properties and their relationship to the oyster
1001 disease MSX in Delaware Bay, *J. Mar. Res.*, *70*, 279–308.
1002
1003 Warner, J. C., W. R. Geyer, and J. A. Lerczak (2005a), Numerical modeling of an estuary:
1004 A comprehensive skill assessment, *J. Geophys. Res.- Oceans*, *110*, C05001,
1005 doi:10.1029/2004JC002691.
1006
1007 Warner, J. C., C. R. Sherwood, H. G. Arango, and R. P. Signell (2005b), Performance of
1008 four turbulence closure models implemented using a generic length scale method, *Ocean*
1009 *Modelling*, *8*, 81-113, doi:10.1016/j.ocemod.2003.12.003.
1010
1011 Willmott, C. J. (1981), On the validation of models, *Phys. Geogr.*, *2*, 184-194,
1012 doi:10.1080/02723646.1981.10642213.
1013
1014 Xiao, Y., and M. A. M. Friedrichs (2014a), Using biogeochemical data assimilation to
1015 assess the relative skill of multiple ecosystem models: effects of increasing the
1016 complexity of the planktonic food web. *Biogeosciences*, *11*, 3015-3030, doi:10.5194/bg-
1017 11-3015-2014.
1018
1019 Xiao, Y. and M. A. M. Friedrichs (2014b), The assimilation of satellite-derived data into
1020 a one-dimensional lower trophic level marine ecosystem model. *J. Geophys. Res.-Oceans*,
1021 *119*, 2691-2712, doi:10.1002/2013JC009433.

1022 Xu, J., and R. R. Hood (2006), Modeling biogeochemical cycles in Chesapeake Bay with
1023 a coupled physicalebiological model, *Estuar. Coast. Shelf. S.*, 69, 19-46, doi:
1024 10.1016/j.ecss.2006.03.021
1025
1026 Xu, J., R. R. Hood, and S. Y. Chao (2005), A simple empirical optical model for
1027 simulating light attenuation variability in a partially mixed estuary, *Estuaries*, 28, 572-
1028 580, doi:10.1007/BF02696068.
1029
1030 Xu, J., W. Long, J. D. Wiggert, L. W. J. Lanerolle, C. W. Brown, R. Murtugudde, and R.
1031 R. Hood (2012), Climate Forcing and Salinity Variability in Chesapeake Bay, USA,
1032 *Estuar. Coast*, 35, 237–261, doi:10.1007/s12237-011-9423-5.
1033
1034 Xue, Z., R. He, K. Fennel, W-J. Cai, S. Lorhenz, C. Hopkinson, 2013, Modeling Seasonal
1035 and Interannual Variability of Circulation and Biogeochemical Processes in the Gulf of
1036 Mexico., *Biogeosciences*, 10, 7219–7234, doi:10.5194/bg-10-7219-2013
1037
1038 Yang, Q., H. Tian, M.A.M. Friedrichs, M. Liu, X. Li, and J. Yang (2014a), Hydrological
1039 responses to climate and land-use changes along the North American east coast: A 110-
1040 Year historical reconstruction. *J. Amer. Water Res. Assoc.* ,1-21, doi:10.1111/jawr.12232.
1041
1042 Yang, Q., H. Tian, M.A.M. Friedrichs, C. Hopkinson, C. Lu (2014b), Increased nitrogen
1043 export from eastern North America to the Atlantic Ocean due to climatic and

- 1044 anthropogenic changes during 1901-2008. Submitted to this special issue of *J. of*
1045 *Geophys. Res – Biogeosciences*, July 2014.
1046

1047 **Table 1:** Willmott Skill of Model Temperature, Salinity, NO₃, NH₄, PON, DON,
 1048 Chlorophyll and Dissolved Oxygen
 1049

	Upper Bay	Middle Bay	Lower Bay	All (temporal)	All (spatial)
Temperature	0.99	0.99	1.00	1.00	1.00
Salinity	0.87	0.94	0.92	0.99	1.00
NO ₃	0.84	0.74	0.40	0.77	0.99
NH ₄	0.46	0.64	0.71	0.65	0.87
PON	0.32	0.39	0.54	0.52	0.88
DON	0.36	0.40	0.41	0.36	0.96
Chlorophyll	0.36	0.43	0.54	0.49	0.94
DO	0.93	0.98	0.96	0.97	0.97

1050

1051 **Table 2:** Comparison of Chesapeake Bay Nitrogen Fluxes (10^9 g-N y^{-1})
 1052

		Historical estimates (1975-1990)	DLEM-ROMS-ECB Model ¹ (2001-2005)
Total Nitrogen input from river		134 ²	
	DIN	-	96 ± 49
	TON	-	58 ± 22
Burial	Stem + Trib	53 ²	46 ± 10
	Stem	21 ³	22 ± 4
Denitrification ⁴	Stem + Trib	40 ²	34 ± 10
	Stem	23 ³	22 ± 9
Net ecosystem productivity		54 ³	74 ± 23
Total Nitrogen export to ocean			
	DIN	3 ³	8 ± 8
	TON	78 ³	91 ± 36

1053 ¹From this study

1054 ²From data derived estimates of *Boynton et al.* [1995]

1055 ³From data derived estimates of *Kemp et al.* [1997]

1056 ⁴Includes both water column and sediment denitrification

1057 ⁵Calculated from TON budget

1058 **Table 3:** Comparison of Freshwater Discharge (km^3y^{-1}), DIN flux (10^9g-N y^{-1}) and TON
 1059 flux (10^9g-N y^{-1}) to Chesapeake Bay
 1060

	DLEM <i>Yang et al. [2014a]</i>	CBP WM* <i>Shenk and Linker [2013]</i>
<i>Freshwater discharge:</i>		
2001	48	55
2002	50	57
2003	144	138
2004	112	106
2005	76	81
mean 2001-2005	86 ± 41	87 ± 35
mean 1985-2005	63 ± 22	75
<i>DIN flux:</i>		
2001	55	65
2002	61	73
2003	176	120
2004	112	88
2005	80	84
mean 2001-2005	96 ± 49	86 ± 21
<i>TON flux:</i>		
2001		32
2002	37	33
2003	40	84
2004	87	67
2005	75	49
mean 2001-2005	52	53 ± 21

1061
 1062 *Shenk and Hinson, pers. comm.

1063 **Table 4:** Comparison of Chesapeake Bay Nitrogen Fluxes and Standard Deviations
 1064 (10^9 g-N y^{-1}) Obtained Using Estuarine Biogeochemical Model (ROMS-ECB; this study)
 1065 and Regional Shelf Biogeochemical Model (USECoS; *Friedrichs et al., in prep. for this*
 1066 *issue*].
 1067

	ROMS-ECB (2001-2005)	USECoS (2004-2008)
river input DIN	96 ± 50	82 ± 16
river input TON	58 ± 22	75 ± 16
Burial	46 ± 10	5 ± 1
Denitrification ³	34 ± 10	6 ± 1
DIN export to ocean	8 ± 8	49 ± 10
TON export to ocean	91 ± 36	56 ± 11

1068 **Figure Captions**

1069 **Figure 1:** Chesapeake Bay (a) model grid and bathymetry, and (b) map illustrating
1070 location of riverine inputs (magenta dots), Thomas Point Light Buoy used for wind
1071 forcing (yellow triangle) and EPA Chesapeake Bay Program Water Quality Monitoring
1072 Stations in the upper (red circles), middle (green circles), and lower (blue circles) Bay.
1073 The black line in (a) denotes the edge of the Bay interior, over which the Bay-wide
1074 budget numbers are computed. The black line in (b) shows the stations along the trench
1075 of the Bay used in Figs. 3, 6, 8.

1076

1077 **Figure 2:** Schematic of the land-estuarine ocean biogeochemical modeling system.
1078 The nitrogen cycle of the estuarine model was detailed illustrated.

1079

1080 **Figure 1:** Observed and simulated seasonal temperature from 2001-2005. Left panels:
1081 temperature along the trench with background color representing the simulation and
1082 circles showing the observations. Right panels: modeled vs. observed temperature at
1083 coincident times and locations. Panels from top to bottom: winter (Dec-Feb); spring
1084 (Mar-May); summer (Jun-Aug) and fall (Sep-Nov). Gray dashed lines in (a) denote the
1085 boundaries of the upper, middle and lower Bay. Stations from upper Bay to lower Bay
1086 are: CB2.1, CB2.2, CB3.1, CB3.2, CB3.3C, CB4.1C, CB4.2C, CB4.3C, CB5.1, CB5.2,
1087 CB5.3, CB5.4, CB5.5, CB6.1, CB6.2, CB6.3, CB7.3, CB7.4.

1088

1089 **Figure 2:** Observed and simulated mean monthly depth-averaged temperature from
1090 2001-2005 in the upper (a), middle (b), and lower (c) Bay. Vertical bars represent ± 1
1091 standard deviation.

1092

1093 **Figure 5:** Taylor (a) and Target (b) diagrams illustrating model skill for hydrodynamic
1094 and biogeochemical fields. Squares represent temporal model skill and circles represent
1095 spatial model skill.

1096

1097 **Figure 6:** As in Figure 3, except for salinity.

1098

1099 **Figure 7:** Observed and simulated monthly salinity from 2001-2005 in the upper (a),
1100 middle (b), and lower (c) Bay. Error bars are ± 1 standard deviations.

1101

1102 **Figure 8:** Observed and simulated climatological (average over five years)
1103 biogeochemical fields from 2001-2005. Panels from top to bottom: $\text{NO}_2 + \text{NO}_3$, NH_4 ,
1104 PON, DON, chlorophyll, and oxygen. Left panels: concentrations along the trench with
1105 background color representing the simulation and circles showing the observations. Right
1106 panels: vertically integrated observed and simulated concentrations at stations shown in
1107 Figure 1b with error bars showing ± 1 standard deviation relative to the 5-year mean.

1108 Gray dashed lines in (a) denote the boundaries of the upper, middle and lower Bay.

1109

1110 **Figure 9:** Observed and simulated vertically integrated monthly biogeochemical fields
1111 averaged over 2001-2005. Error bars are ± 1 standard deviations. Panels from left to right:

1112 NO₂ + NO₃, NH₄, PON, DON, chlorophyll and oxygen. Panels from top to bottom:
1113 upper, middle and lower Bay.

1114

1115 **Figure 10:** Comparison between five-year (2001-2005) averaged sea surface chlorophyll
1116 from (a) SeaWiFS and (b) model simulation. Skill assessment is illustrated by (c)
1117 unbiased RMSD, and (d) Willmott skill together with histograms of (e) unbiased RMSD
1118 and (f) Willmott skill.

1119

1120 **Figure 11:** The nitrogen budget for 2001-2005 in the Chesapeake Bay from our modeling
1121 system (unit: 1×10^9 g-N y⁻¹). The exchange of DIN/PON between the internal Bay and
1122 exterior ocean was estimated using the mean velocity and DIN/PON concentration fields
1123 averaged daily at a cross section of Bay mouth (red line in Figure 1a). Net ecosystem
1124 productivity (NEP) was estimated from the TON budget as in *Kemp et al.* [1997].

1125

1126 **Figure 12:** (a) Freshwater discharge for the 2001-2005 period. Multiple years average
1127 (1980-2008) with the standard deviation was shown (grey solid and dashline); (b)
1128 Interannual variability of nitrogen fluxes computed for the 2001-2005 analysis period.

1129

1130

1131

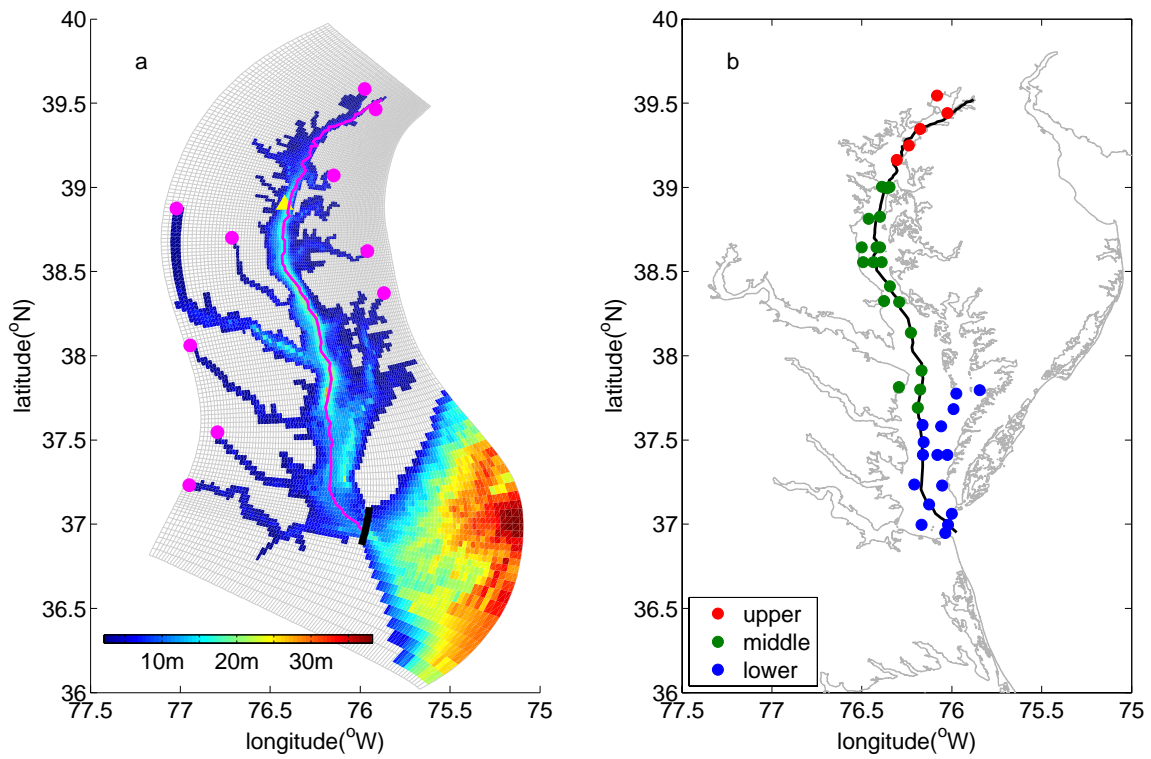


Figure 1: Chesapeake Bay (a) model grid and bathymetry, and (b) map illustrating location of riverine inputs (magenta dots), Thomas Point Light Buoy used for wind forcing (yellow triangle) and EPA Chesapeake Bay Program Water Quality Monitoring Stations in the upper (red circles), middle (green circles), and lower (blue circles) Bay. The black line in (a) denotes the edge of the Bay interior, over which the Bay-wide budget numbers are computed. The black line in (b) shows the stations along the trench of the Bay used in Figs. 3, 6, 8.

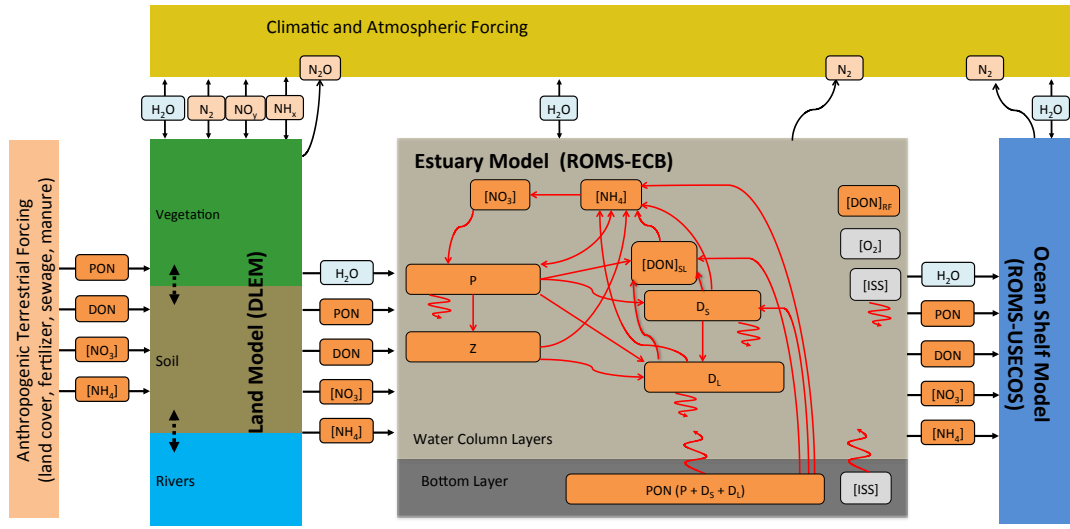


Figure 2: Schematic of the nitrogen components of the land-estuarine-ocean biogeochemical modeling system (ROMS-ECB-DLEM).

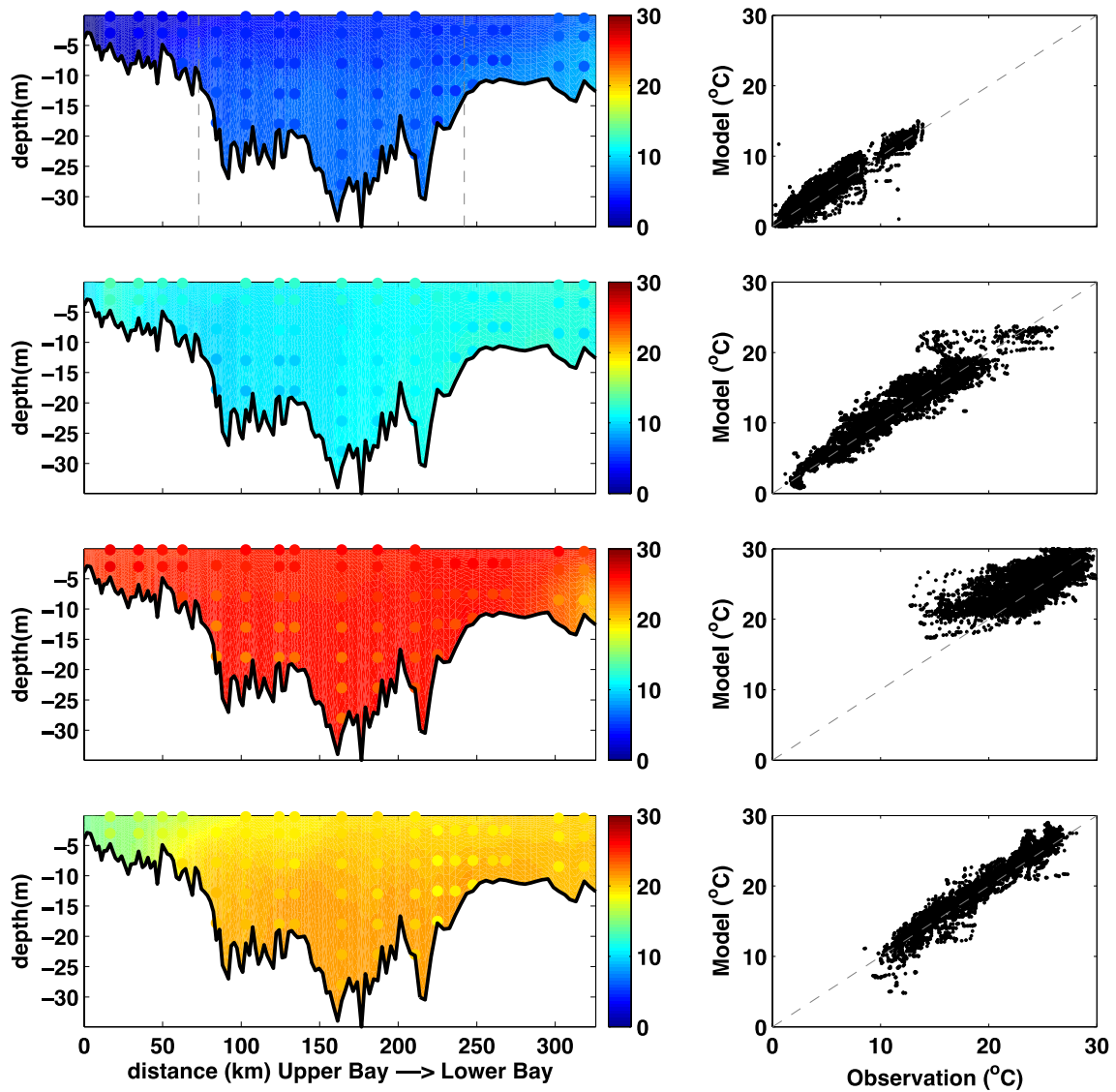


Figure 3: Observed and simulated seasonal temperature from 2001-2005. Left panels: temperature along the trench with background color representing the simulation and circles showing the observations. Right panels: modeled vs. observed temperature at coincident times and locations. Panels from top to bottom: winter (Dec-Feb); spring (Mar-May); summer (Jun-Aug) and fall (Sep-Nov). Gray dashed lines in (a) denote the boundaries of the upper, middle and lower Bay. Stations from upper Bay to lower Bay are: CB2.1, CB2.2, CB3.1, CB3.2, CB3.3C, CB4.1C, CB4.2C, CB4.3C, CB5.1, CB5.2, CB5.3, CB5.4, CB5.5, CB6.1, CB6.2, CB6.3, CB7.3, CB7.4.

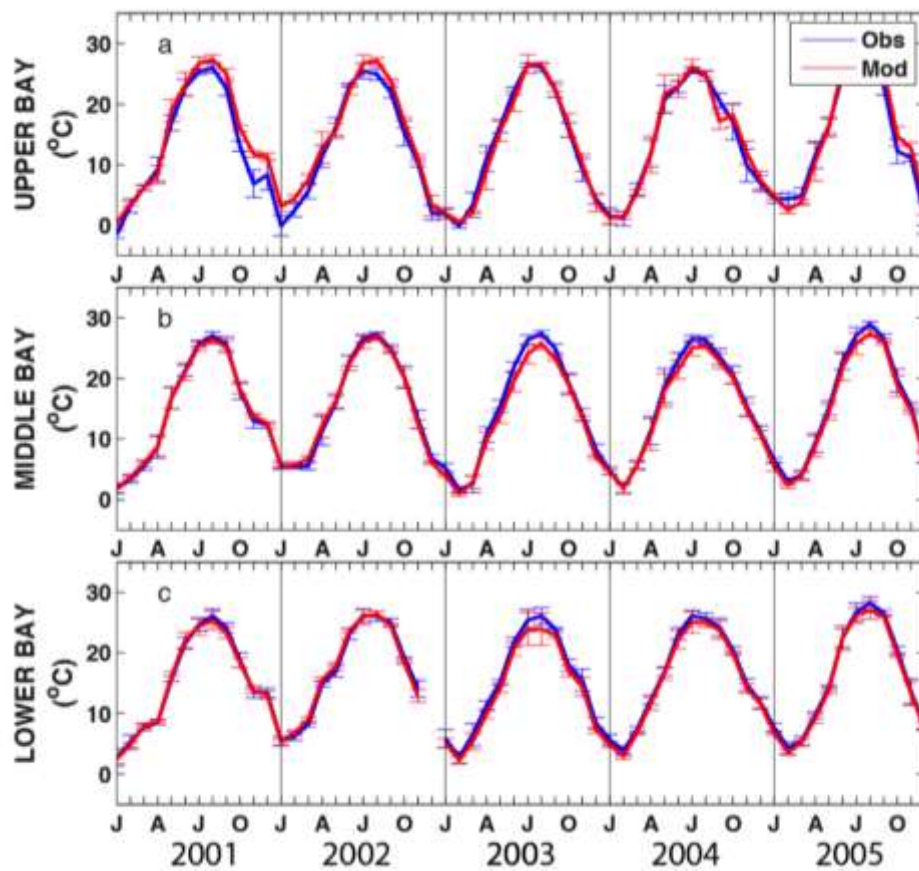


Figure 4: Observed and simulated mean monthly depth-averaged temperature from 2001-2005 in the upper (a), middle (b), and lower (c) Bay. Vertical bars represent ± 1 standard deviation.

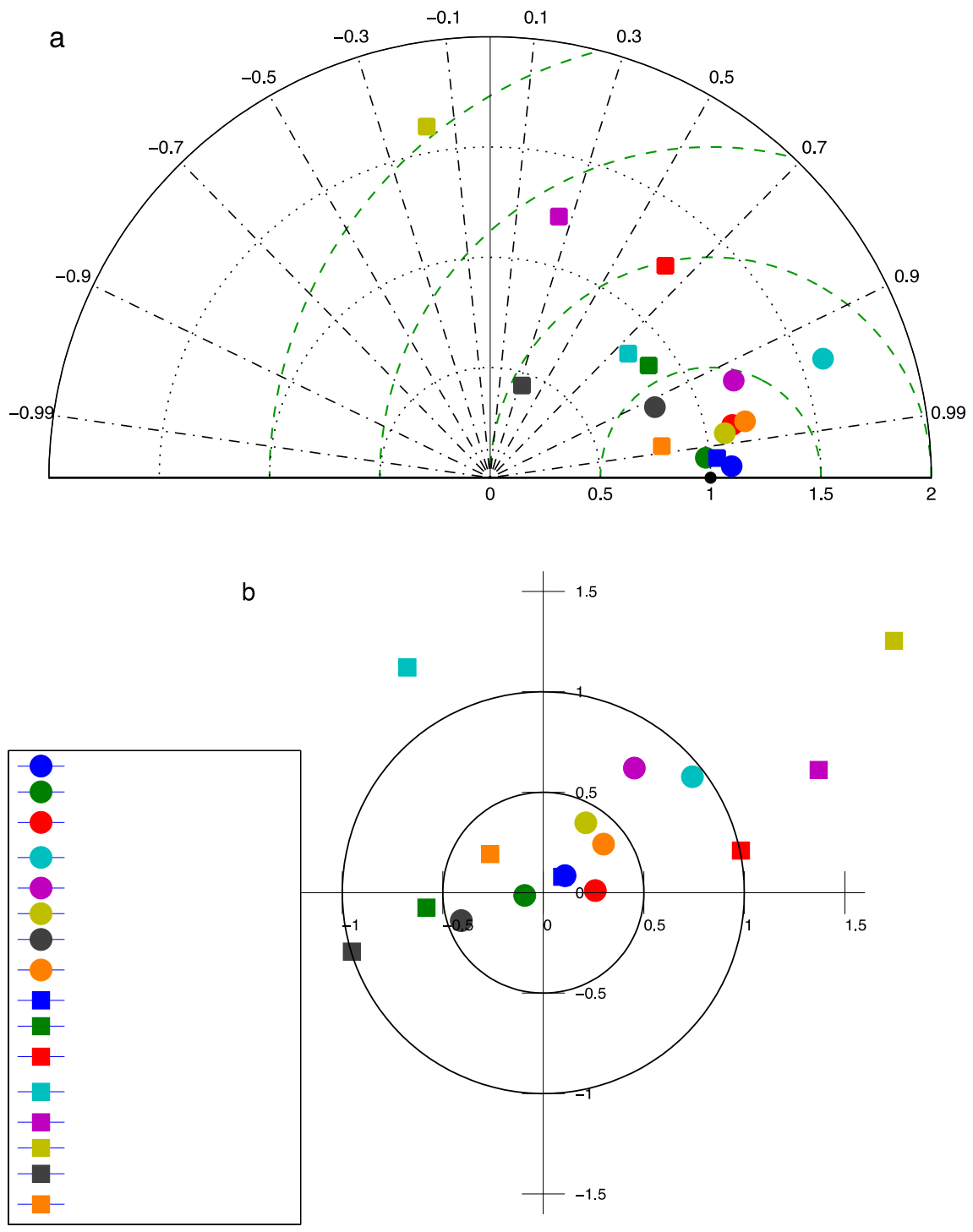


Figure 5: Taylor (a) and Target (b) diagrams illustrating model skill for hydrodynamic and biogeochemical fields. Squares represent temporal model skill and circles represent spatial model skill.

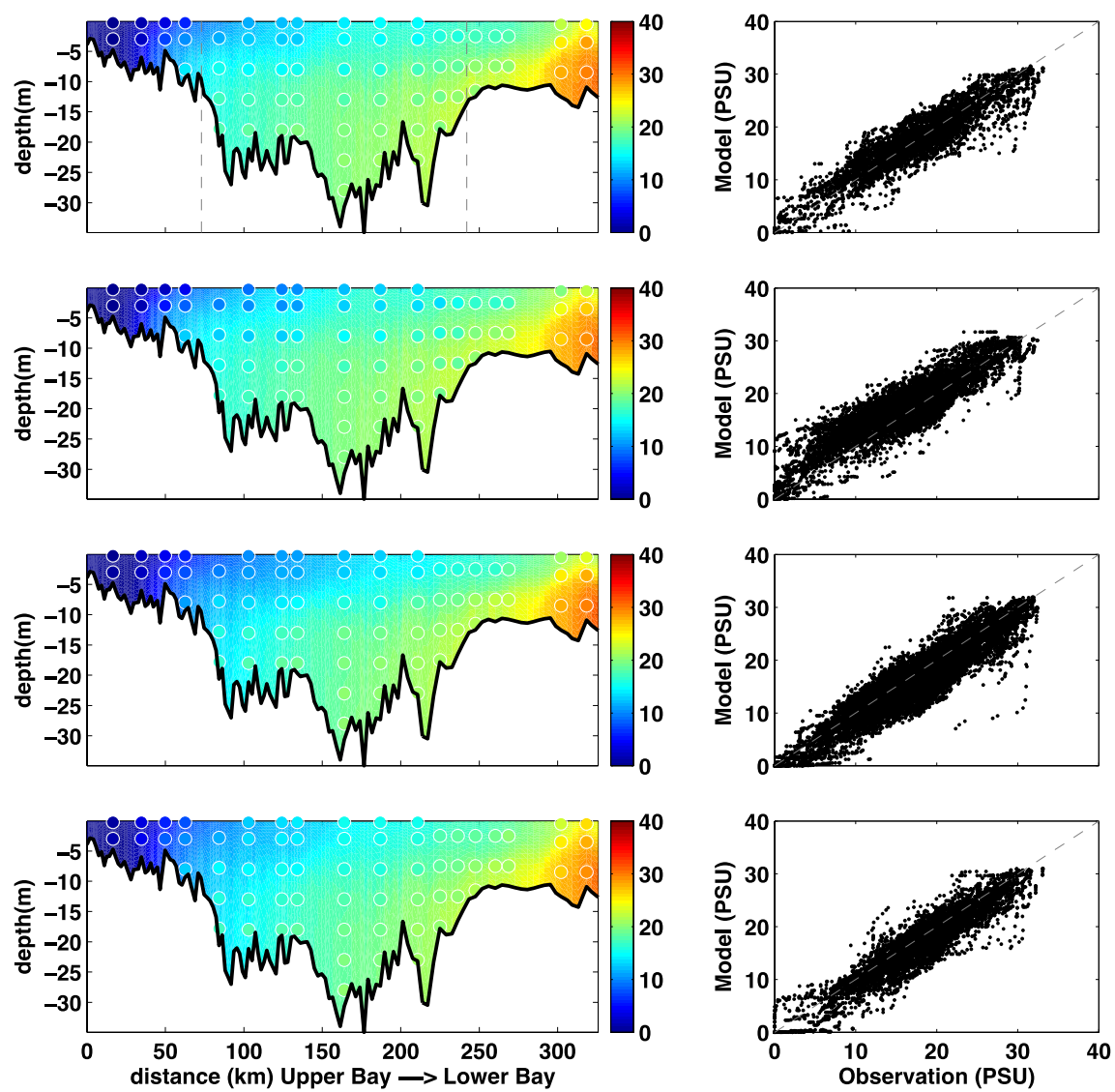


Figure 6: As in Figure 3, except for salinity.

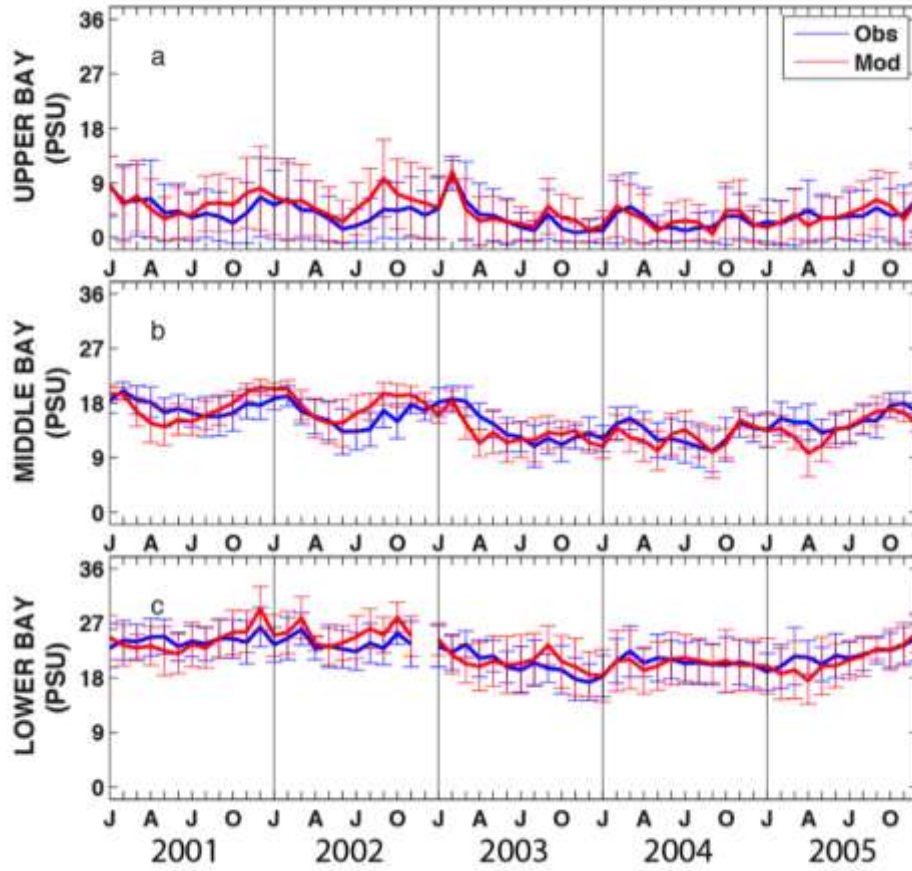


Figure 7: Observed and simulated monthly salinity from 2001-2005 in the upper (a), middle (b), and lower (c) Bay. Error bars are ± 1 standard deviations.

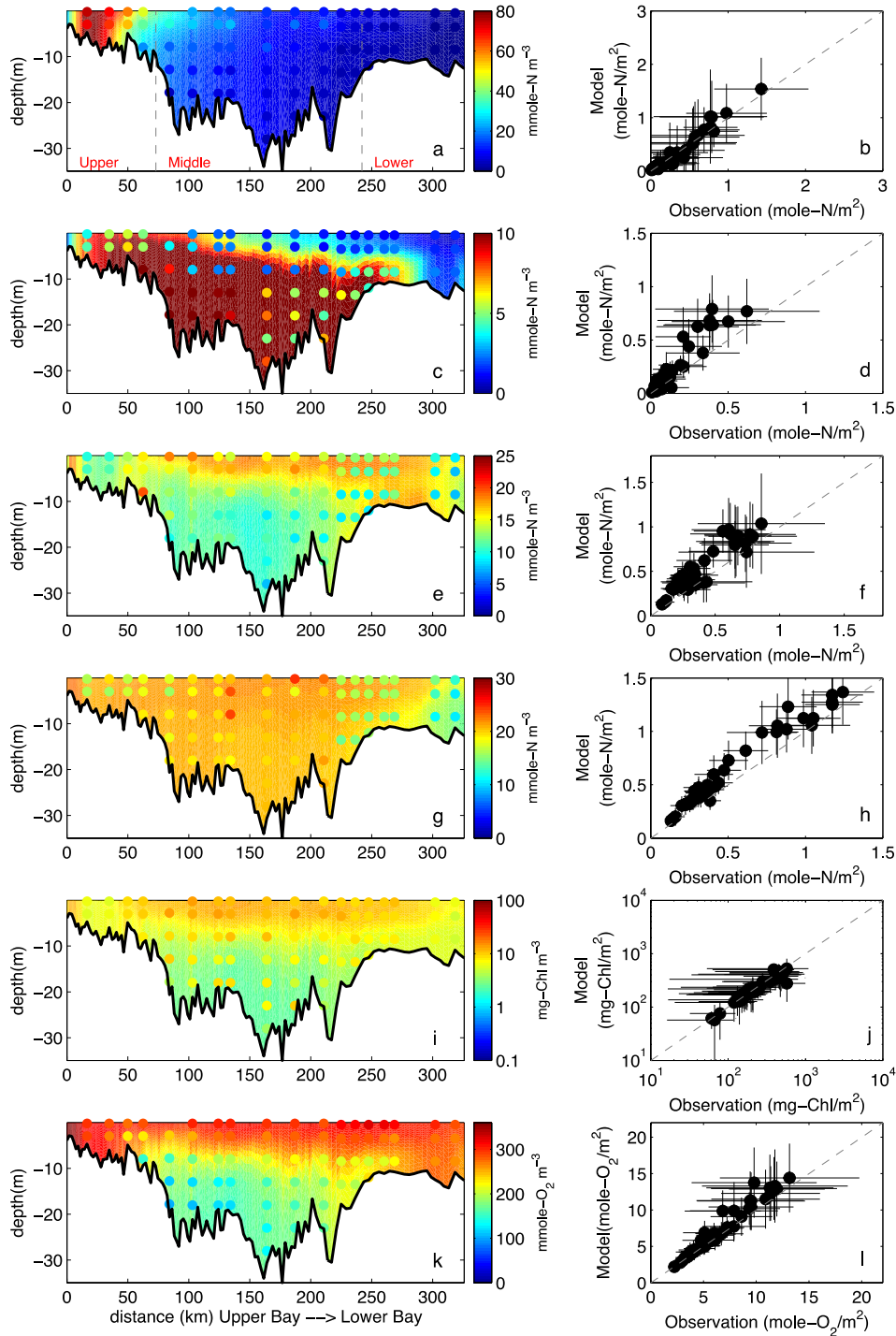


Figure 8: Observed and simulated climatological (average over five years) biogeochemical fields from 2001-2005. Panels from top to bottom: $\text{NO}_2 + \text{NO}_3$, NH_4 , PON, DON, chlorophyll, and oxygen. Left panels: concentrations along the trench with background color representing the simulation and circles showing the observations. Right panels: vertically integrated observed and simulated concentrations at stations shown in Figure 1b with error bars showing ± 1 standard deviation relative to the 5-year mean. Gray dashed lines in (a) denote the boundaries of the upper, middle and lower Bay.

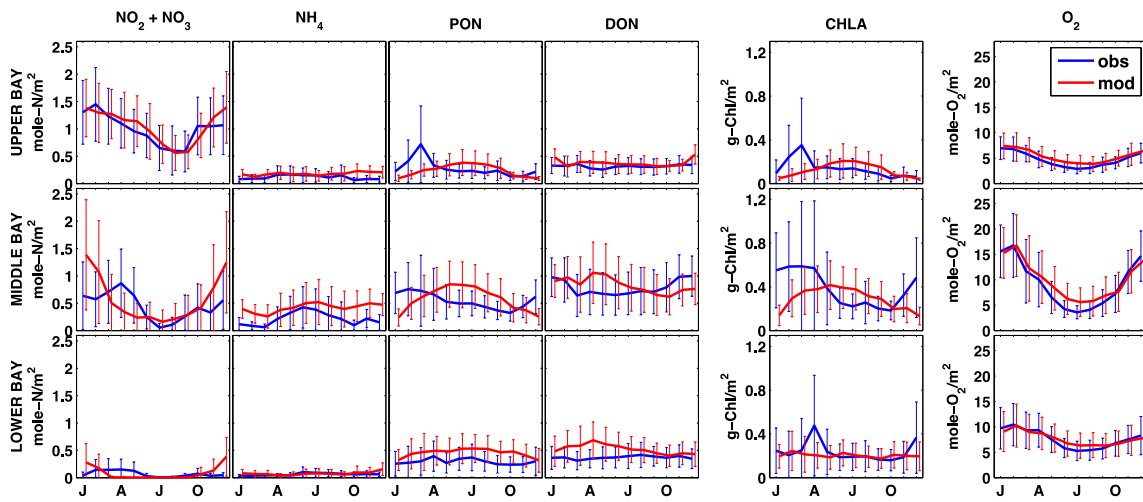


Figure 9: Observed and simulated vertically integrated monthly biogeochemical fields averaged over 2001-2005. Error bars are ± 1 standard deviations. Panels from left to right: $\text{NO}_2 + \text{NO}_3$, NH_4 , PON, DON, chlorophyll and oxygen. Panels from top to bottom: upper, middle and lower Bay.

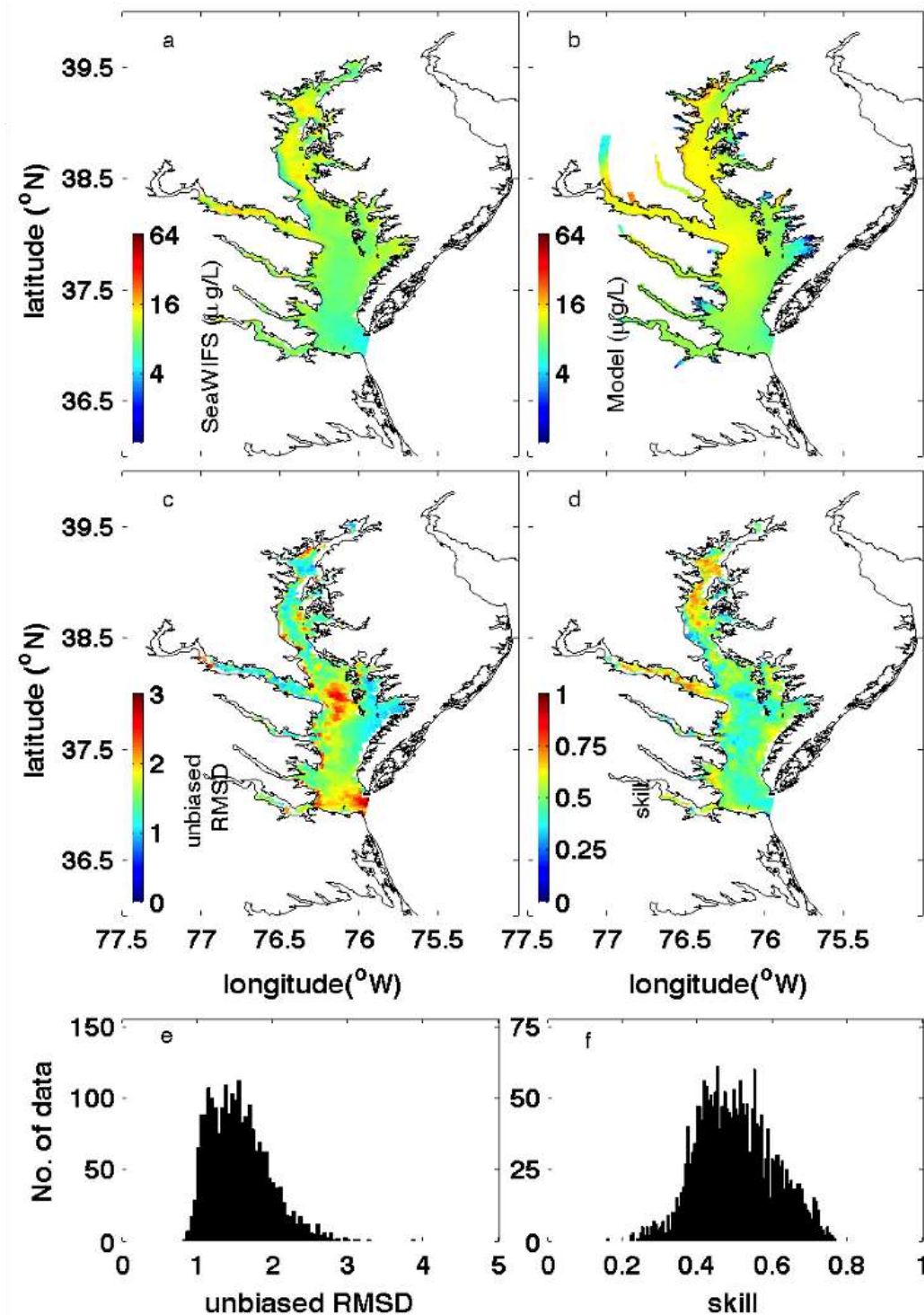


Figure 10: Comparison between five-year (2001-2005) averaged sea surface chlorophyll from (a) SeaWiFS and (b) model simulation. Skill assessment is illustrated by (c) unbiased RMSD, and (d) Willmott skill together with histograms of (e) unbiased RMSD and (f) Willmott skill.

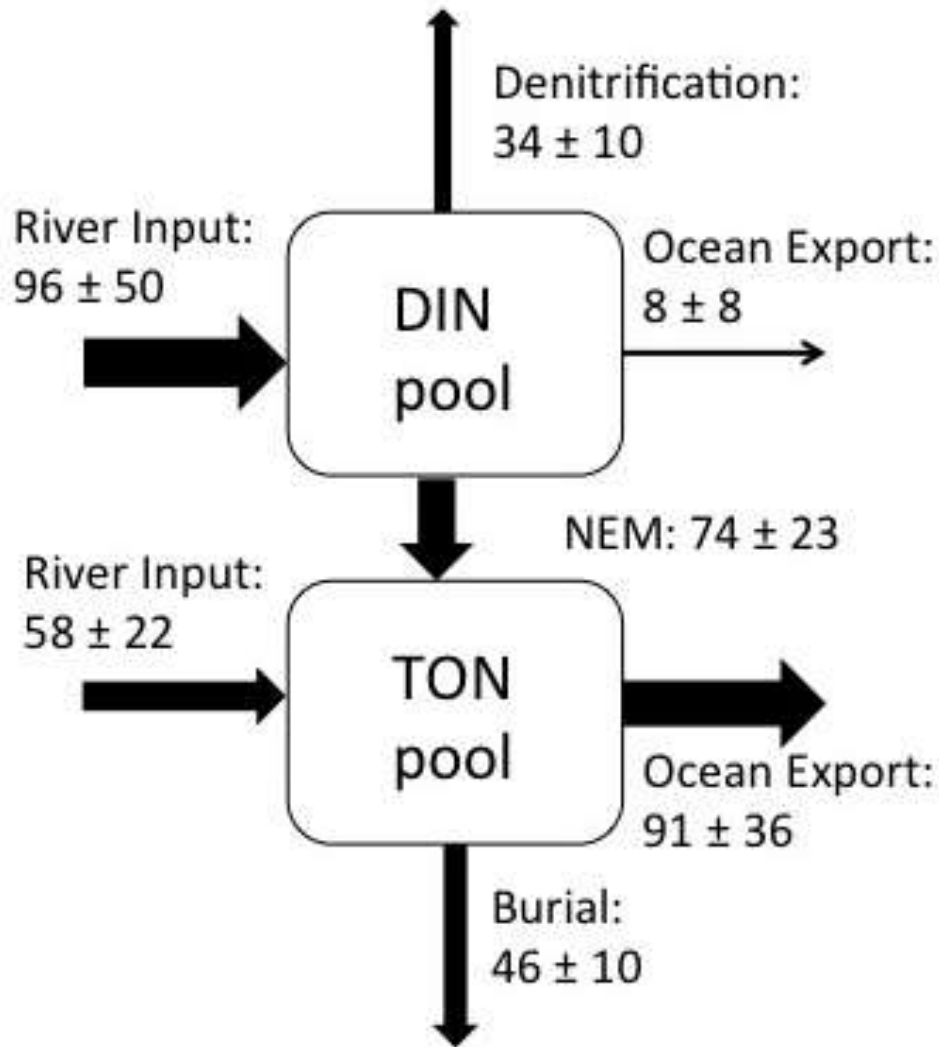


Figure 11: The nitrogen budget for 2001-2005 in the Chesapeake Bay from our modeling system (unit: 1×10^9 g-N y^{-1}). The exchange of DIN/PON between the internal Bay and exterior ocean was estimated using the mean velocity and DIN/PON concentration fields averaged daily at a cross section of Bay mouth (red line in Figure 1a). Net ecosystem productivity (NEP) was estimated from the TON budget as in *Kemp et al.* [1997].

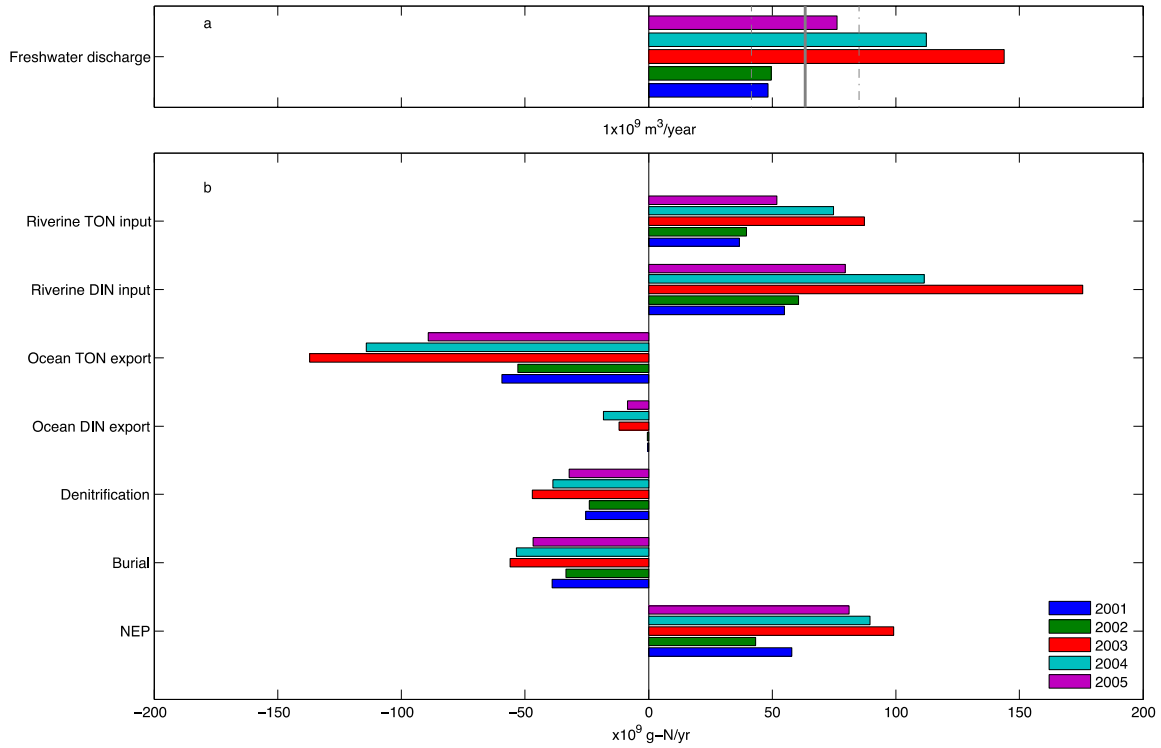


Figure 12: (a) Mean freshwater discharge for each simulation year, with the long-term DLEM mean discharge (1980-2008; grey solid line) and standard deviation (gray dashed line) included for reference; (b) Interannual variability of nitrogen fluxes computed for each of the simulation years.